

A PARAMETRIC OPTIMIZATION OF LATTICE
STRUCTURE HEAT SINKS: AN INTEGRATED
COMPUTATIONAL AND EXPERIMENTAL
APPROACH

By

TURNER MCCOY

Bachelor of Science in Mechanical Engineering

Technology

Oklahoma State University

Stillwater, Oklahoma

2021

Submitted to the Faculty of the
Graduate College of the
Oklahoma State University
in partial fulfillment of
the requirements for
the Degree of
MASTER OF SCIENCE
May, 2023

A PARAMETRIC OPTIMIZATION OF LATTICE
STRUCTURE HEAT SINKS: AN INTEGRATED
COMPUTATIONAL AND EXPERIMENTAL
APPROACH

Thesis Approved:

Hitesh Vora

Thesis Adviser

Aaron Alexander

Chulho Yang

ACKNOWLEDGEMENTS

I would like to express my sincere gratitude and appreciation to all those who have supported and contributed to the completion of this research.

Firstly, I am grateful to the Oklahoma Center for the Advancement of Science and Technology (OCAST) for providing the necessary funding to undertake this research project. The OCAST grant has been critical in enabling the successful completion of this thesis.

I would like to express my deepest appreciation to my advisor, Dr. Hitesh Vora, for his invaluable guidance, mentorship, and support throughout the research process. His unwavering commitment to my academic and personal growth has been integral to my success. I also want to extend my profound thanks to Dr. Alexander and Dr. Yang for serving on my committee and providing their expertise, and guidance.

Lastly, I express my gratitude to my family and friends for their unwavering love, support, and encouragement throughout my academic journey. Their belief in me and their constant encouragement has been a constant source of motivation.

Name: TURNER MCCOY

Date of Degree: MAY, 2023

Title of Study: A PARAMETRIC OPTIMIZATION OF LATTICE STRUCTURE HEAT SINKS: AN INTEGRATED COMPUTATIONAL AND EXPERIMENTAL APPROACH

Major Field: ENGINEERING TECHNOLOGY

Abstract: Lattice structures have frequently been investigated for their unique mechanical and thermal properties and have been optimized for better performance for these characteristics. Their mechanical properties have shown amazing results and have been thoroughly investigated in many comprehensive studies. However, trending research is now investigating their thermal properties, specifically for heat dissipation or insulation applications. To further build on this research, our approach considers the design, manufacturing, modeling, and characteristics to develop a lattice structure optimized for heat sink applications. Utilizing efficient technologies in additive manufacturing, we employ fused deposition modeling (FDM) as the method of fabrication. FDM is currently the most popular method of additive manufacturing due to its simplicity and price. A microscopy analysis of a PLA-copper-infused filament verified that parts from a low-cost FDM printer can produce parts over 80% copper after debinding and sintering heat treatments. Using a design of experimentations, we have identified 3 variables in lattice structures, strut diameter, cell size, and cell type, and optimized these heat sinks for evaluation parameters of heat sinks. Using a statistical analysis software Design Expert, we have designed and run multiple heat sinks through computational fluid dynamics (CFD) simulations to predict heat transfer to analyze the trends of these variables to develop a heat sink. Our results found three optimized lattice structure heat sinks that we validated through CFD. Our study found characteristics that can be used in further research and testing to develop low-cost additively manufactured heat sinks. The method we utilized can also be used for future research for efficiently optimizing heat sinks.

TABLE OF CONTENTS

Chapter	Page
I. INTRODUCTION.....	1
1.1 Problem Statement.....	1
1.2 Objectives	3
II. REVIEW OF LITERATURE.....	4
Heat Sinks	4
Lattice Structures	8
Additive Manufacturing.....	11
Optimization	13
III. DESIGN OF EXPERIMENTS	18
Introduction.....	18
Selection of Parameters and Modeling	20
Design of Experiments.....	23
IV. OPTIMIZATION AND DISCUSSION	25
Optimization Methodology.....	25
Optimization Process	26
Validation.....	33
V. MANUFACTURING.....	37
Introduction.....	37
Shrinkage Study	42
Microscopy Analysis	45

Chapter	Page
VI. CONCLUSION.....	50
Conclusion	50
Future Work	51
REFERENCES	53

LIST OF TABLES

Table	Page
1. Design of Experiments Parameters.....	21
2. Requested Lattice Structures from the DOE.....	22
3. Results from DOE Simulations.....	24
4. Optimization #1 Criteria.....	27
5. Results from Optimization #1.....	27
6. Optimization #2 Criteria.....	29
7. Results from Optimization #2.....	30
8. Optimization #3 Criteria.....	32
9. Results from Optimization #3.....	32
10. CFD Results of Optimized Heat Sinks.....	36
11. Percent Difference Between DOE and CFD.....	36
12. 3D Printer Settings for Copper Filament.....	39
13. Shrinkage Study Measurements.....	43
14. Final Shrinkage Ratios.....	44
15. Results from EDS Scan.....	49

LIST OF FIGURES

Figure	Page
1. Four Elements of Characterization	3
2. Styles of Heat Sinks [8]	7
3. Examples of Lattice Structure Unit Cells [14].....	9
4. Additive Manufacturing Processes [23].....	12
5. Yun's Graded lattice channel designs [36].....	15
6. Yan's X-lattice Structure Integrated with a Honeycomb Structure [37]	16
7. Heat Sinks from Vaissier's Study [38].....	17
8. Research Methodology Flowchart	19
9. Side View of 'X' Lattice Structure	20
10. Optimized Lattice Structure #1: Cell Size of 15.771 mm [43].....	34
11. Optimized Lattice Structure #2 Cell Size of 16.608 mm [43]	35
12. Optimized Lattice Structure #3 Cell Size of 18.404 mm [43]	35
13. 3D Printer Setup.....	38
14. Copper Debind and Sintering Temperature and Times [44].....	40
15. Copper Samples in Crucible Before Debinding.....	41
16. Copper Parts in Crucible in Furnace	41
17. Copper Samples Buried in Talc and Sintering Carbon.....	42
18. Printed, Debinded, and Sintered Copper Samples	43
19. Scaled Heat Sink in Slicing Software	45
20. SEM Image of Copper Filament	46
21. SEM Image of Polished Copper Filament	47
22. SEM Image of Debinded Copper Sample.....	48
23. SEM Image of Sintered Copper Sample.....	48
24. Graph of EDS Scan.....	49

CHAPTER I

INTRODUCTION

1.1 Problem Statement

Thermal management is an increasingly important sector of the electronics industry and will continue to grow with the market's demand for products with increased functionality in a smaller package. This challenge comes with the need to remove the wasted energy in the form of heat from the system. Optimizing heat sinks for better natural convection cooling per volume means fewer components for cooling or at least smaller and potentially lighter ones. This is a major driving factor in many industries such as aerospace where weight constraints are critical. Optimization without a clear scope can be a very inefficient process. Using numerical methods can drastically reduce the time for optimization while simulation software can eliminate prototyping and testing expenses.

Many researchers have attempted heat sink optimization using various geometries. Plate fin and pin fin heat sinks are some of the most popular designs that have been investigated several times. Recently cellular materials like stochastic foams and lattices have been studied for their mechanical and thermal properties. Mechanically, these structures are excellent at distributing internal stresses allowing them to have high strength-to-weight ratios. Due to their high surface area-to-volume ratio, they are natural candidates for heat dissipation applications as well. Stochastic foams have impressive

surface area-to-volume ratios and allow for great conduction of heat but are irregular by nature and can be difficult to repeat results. Lattices offer similar characteristics and have an organized geometry that can be modeled accurately. These models offer the opportunity to utilize modeling technologies like computational fluid dynamics (CFD) to quickly understand their thermal characteristics.

The goals of this research are to identify and investigate which characteristics of lattice structures lead to improved heat sink performance and evaluate the method used for optimization. Using a Design of Experiments will efficiently identify trends and indicate what criteria to optimize for. Computational fluid dynamics (CFD) is used as a method of validating the results from this study efficiently before a significant stake is invested in manufacturing and testing the heat sinks.

To guide this research, we focused on 4 elements of characterization. Performance, modeling, design, and manufacturing. Each one is interconnected and contributes to a well-rounded approach. Our manufacturing scope was narrowed to heat sinks manufacturable by FDM printers. This came with some design and materials limitations that will be discussed later. Designing the lattices required a significant amount of trial and error while considering design for additive manufacturing principles and compatible files for simulations. Modeling played a significant role in this research not only in time but in collecting data. Tools like CFD and optimization software allowed us to model results in an efficient matter. Throughout the research, a diverse amount of data was collected. Evaluating the performance of data points from CFD to the microscopy analysis to the optimization required mindful consideration of all aspects of

the research. The figure below illustrates how all elements of this research played into the characterization of the results.

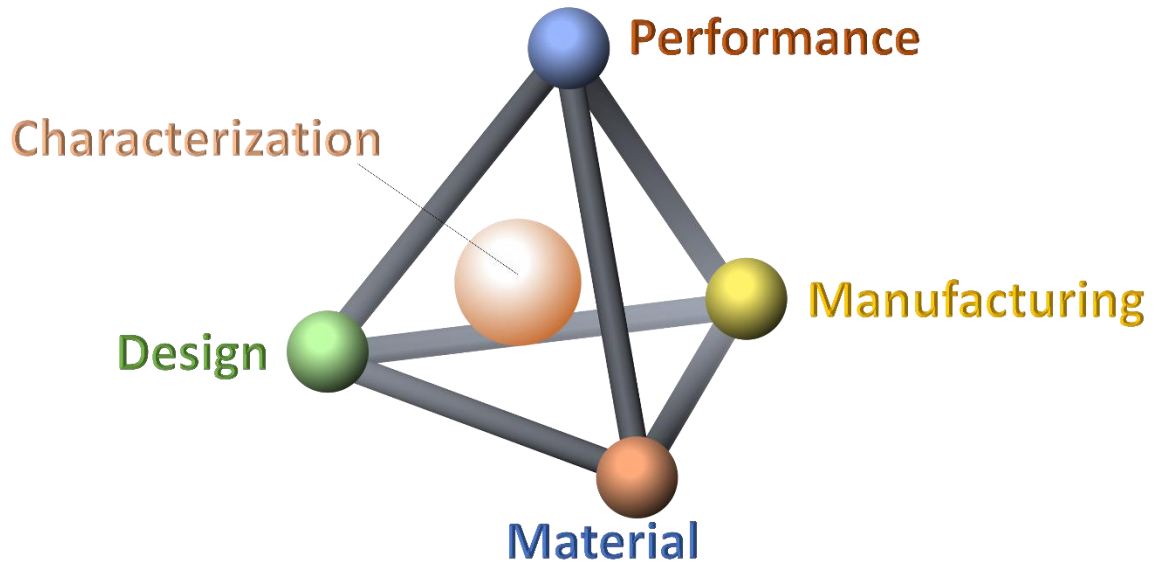


Figure 1: Four Elements of Characterization

1.2 Objectives

Objective 1: Identify modeling characteristics of lattice structures to be used as variables for the design of experiments. Perform the design of the experiment using CFD to efficiently collect data and import the data for optimization. After progressively identifying key parameters, optimize with strict constraints to yield a small number of solutions. Model and validate solutions through CFD.

Objective 2: Identify and evaluate PLA-Copper infused filament for fabricating low-cost heat sinks. Determine shrinkage ratio for dimensionally accurate final parts. Investigate the composition of the material at all points of the manufacturing process (raw filament, printed, debinded, and sintered) to understand the material properties and how they might affect the heat sink's performance.

CHAPTER II

REVIEW OF LITERATURE

2.1 Heat Sinks

There are currently several different ways of removing excess heat from electronics typically through conduction or convection. The equations for these methods of heat transfer can be found in Eq (1), (2) and (3). Convection is the most significant form of heat removal by a heat sink. Convection occurs when a surface transfers heat into a fluid like air or water. Conduction refers to the heat transfer of two stationary mediums, typically solid objects but can occur with fluids as well. There are two sub-classifications of heat transfer technologies: passive and active. The major difference between the two is that active heat transfer requires an external power source. This is commonly seen as a fan being used as a method to increase the rate of convection in the system. Meaning the fan moves cooler air into the system creating a larger temperature gradient and transferring more heat. With the addition of a fan, a heat sink can handle up to 10 times more power [1]. However, there are some drawbacks when adding a fan to the system. The fan needs a power supply which increases the total power needed for the system and the labor of integrating it into the design. There is also the additional cost of the fan. This may just be a few dollars but if multiple components require active cooling and the product is being mass-produced this could result in a significant loss of profit. Finally,

there is a significant amount of risk being taken when the success of the entire system depends on one component to run continuously.

It is possible to use multiple methods to optimize the removal of heat from the system. Radiation, a less efficient method of heat transfer, is the energy released by matter in the form of photons and electromagnetic waves. The equation for heat transfer via radiation can be found in Eq. 3. Where ε is the emissivity of the object, σ is the Stefan-Boltzmann constant, T_s is the surface temperature of the object and T_{surr} is the temperature of the surrounding.

$$Q_{Conv} = hA(T_s - T_{amb}) \quad (1)$$

$$Q_{Cond} = \frac{kA(T_2 - T_1)}{L} \quad (2)$$

$$Q_{Rad} = \varepsilon\sigma A(T_s^4 - T_{surr}^4) \quad (3)$$

This emissivity value ranges from zero to one and is often the only manipulatable part of this equation to increase heat transfer by radiation. The color black is known to have a higher emissivity value and absorbs and emits radiation much more efficiently. For this reason, you will sometimes see heat sinks painted black. However, radiation is a much smaller portion of the total heat transfer by a heat sink. A mathematical study found that radiation accounts for very little heat transfer when used with a forced convection heat sink (with a fan), but a significantly larger portion for natural convection heat sinks. The study compared forced convection and natural convection heat sinks at typical power inputs. For forced convection heat sinks radiation contributed to about 1% to 5% compared to 10% to 30% for a natural convection heat sink. [2]. While the improvements

might be minor in most scenarios, it is a strategy that can be used when a design requires a slight improvement to meet specifications.

Heat sinks are a specific thermal management device commonly used to remove heat from high-power semiconductor devices such as processors, LEDs, and other hardware that may generate an excessive amount of heat that could be damaging or limit the devices' functionality. Heat sinks function by drawing the heat from the component typically through conduction, then expelling it into the cooling fluid medium, often the air. Aluminum and copper are the two most popular materials for heat sinks because of their high thermal conductivity and cost [3]. Thermal conductivity, k , is a critical aspect of heat transfer via conduction. This value can be thought of as the ability to move heat through the material. For heat sink applications it is important to use a highly conductive material so that heat from the source can be quickly absorbed and distributed in the heat sink so it can be removed.

While heat sink geometry varies greatly, they all possess a common functional feature which is the fins that contact the fluid medium. These fins are typically designed so that they have a high surface area for a greater rate of heat transfer by convection [4]. The two most common types of fins are plate fin and pin fin as seen below in Figure 2. There are numerous ways heatsinks are manufactured today, but the most popular include extrusion, stamping, die casting, and machining. Extrusion, the most popular method, forces material through a die matching the desired 2D cross-section of the heatsink. This is a very cost-effective method but is limited by the geometries it can produce. Stamping is also a low-cost option, that typically produces low-performance heat sinks. They are made from sheet metals that have been cut with a metal stamping die. The stamped part is

often designed for specific applications on a printed circuit board. Die-cast heat sinks are made by pressurizing molten metal into the die. This process yields high-quality parts that can be improved by machining the surface after casting. This process requires a significant investment upfront for the mold; however, parts are produced quickly and at a low cost. Machined heat sinks are made by simply removing material away from a larger block of material until the desired geometry is achieved. This is typically done using CNC machining. This method offers low turnaround and typically high thermal conductivity but has a significant amount of wasted material and can be an expensive process [5] [6] [7]

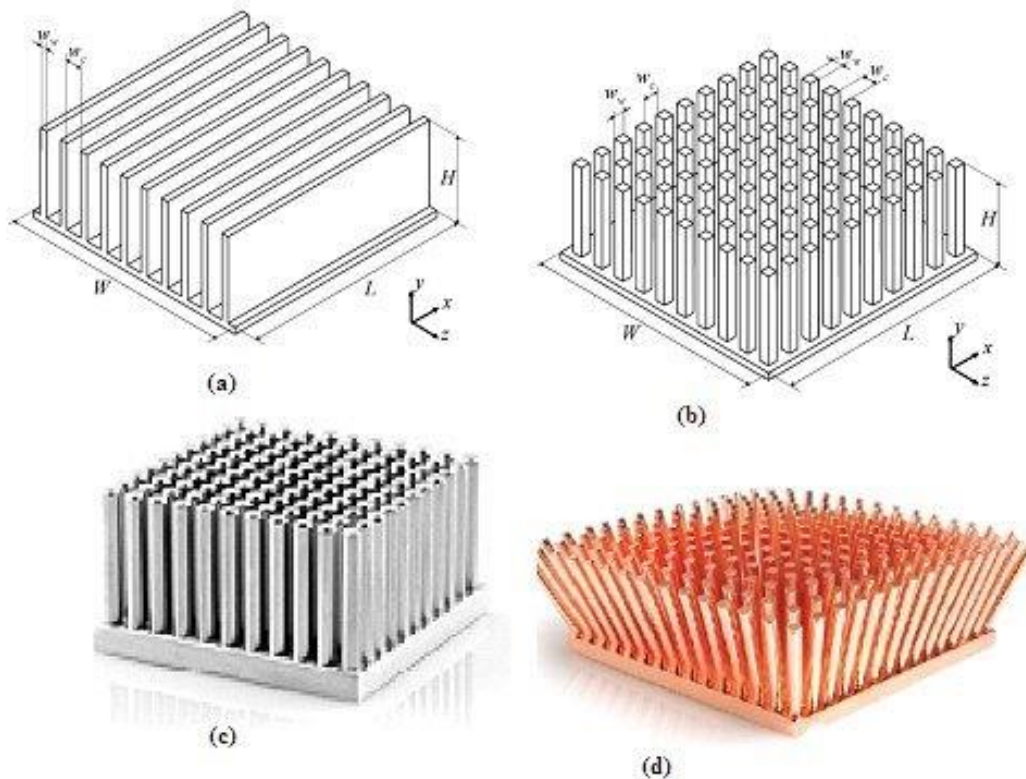


Figure 2: Styles of Heat Sinks [8]

Plate fin heat sinks are typically cheaper to manufacture and design whereas pin fins perform well in different orientations. Both types are very common in the industry. Joo found plate-fine fin heat sinks performed better for total heat dissipation while the pin-finned heat sinks had a higher heat dissipation per mass while occupying the same volume. [9]

According to Expert Market Research, the global heat sink industry was worth about 6.5 billion dollars in 2021 and is expected to grow to 9.5 billion by 2027 [10]. It is estimated that more than 10^9 kWh is used to power fans for forced convection over heat sinks in personal computers alone a year. [11] Therefore, the more efficient natural convection heat sinks become, the fewer devices will require active cooling, and thus less wasted energy and cost savings.

2.2 Lattice Structures

Cellular materials or lattice structures as they are often referred to are a repeated network of cells comprised of strut members and nodes where these members meet [12]. From a mechanical viewpoint, the main benefit of lattice structures is their high compressive strength and lightweight design. Their advantage comes from their easily controllable structural characteristics, load-bearing capacity, and high surface density [13]. The unit cell is the repeated geometry within the lattice structure. Several different unit-cell-type designs have been created and each has different properties, often related to the number of nodes, and struts they have. The figure below shows examples of unit cells.

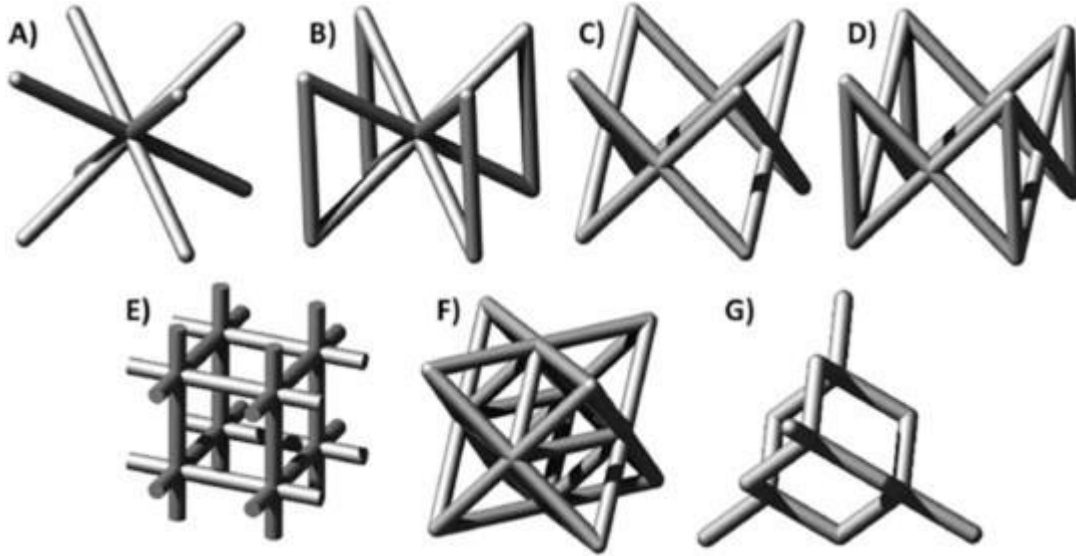


Figure 3: Examples of Lattice Structure Unit Cells [14]

As observed several times by researchers such as Leary & et al. Several different unit cell-type designs have been created and each having different properties, often related to the number of nodes and struts they have. Their mechanical tendencies have been quantified by their Maxwell number, M , which relates the number of struts and nodes in a three-dimensional unit cell to predict a failure type.

$$M = s - 3n + 6 \quad (4)$$

Where s is the number of struts and n is the number of nodes in a unit cell. A Maxwell number of $M < 0$ would not have enough struts to equilibrate external reaction forces without moments existing in lattice nodes. This would result in a cellular structure being defined as bending-dominated. Whereas a unit cell with a Maxwell number of $M \geq 0$ contains enough struts to equilibrate the external forces in tension and compression in the struts, making it stretch-dominated. A stretch-dominated cellular structure typically

displays higher strength whereas a bending-dominated structure would have lower strength but extended plateau stress [15].

Many investigations have been performed on lattice structure mechanical properties [16] [17]. The strategic distribution of stress makes lattice structures great candidates for mechanical optimization and lightweight solutions to engineering problems. As mentioned, the high stiffness-to-weight ratio of lattice structures is particularly attractive for compressive applications. Each cell type distributes forces differently so overarching statements for the mechanical performances cannot be made confidently. Many factors such as unit cell type, strut diameter, node diameter, material, manufacturing process, and imperfections play into the role of AM lattice structures' mechanical strength. Lattice structures have often been compared to stochastic foams since they have similar strengths lightweight and compressions strength. Stochastic foams, which can be open or closed cells are manufactured so that their geometries are random [18]. This leads to the porosity of a stochastic foam being a defining characteristic. Both lattices and stochastic foams have been proposed and studied for multifunction applications. One study directly compared the octet truss lattice to stochastic foams of specified porosities for their thermal dissipation properties. Lattice structures are widely considered a better candidate for optimization because they are repeating and controlled [19]

Lattice structures have become a popular area of research for their heat transfer capabilities in passive and active heat transfer applications [20]. Ho suggests the application of a Rhombi-Octet lattice structure air-cooled heat sinks for high heat flux electronics. [21]. Dixit researched polymer lattice structures heat sinks and compared

them to metal counterparts. She found that while the internal conduction was significantly worse than expected, the heat transfer per weight remained about the same. She also found that the lattice structure with the highest surface area did not show improved performance while the lattice with the lowest surface area had the second-highest rate of heat transfer. She concluded that the architecture played a more significant role in heat transfer than the surface area [22].

2.3 Additive Manufacturing

Additive manufacturing (AM) has become an increasingly popular option for prototyping and low-volume production over the past decade. There are 6 major processes of 3D printing: material extrusion, vat polymerization, powder bed fusion, material jetting, and binder jetting direct. Within these methods can be multiple technologies that utilize the same concept to fabricate parts. Material extrusion, the most common process, creates parts by selectively dispensing material through an orifice. This technology is known as Fused Filament Fabrication (FFF) or more commonly, Fused Deposition Modeling (FDM). Vat polymerization, another popular process occurs when a liquid photopolymer is cured selectively by light. Stereolithography (SLA) and Direct Light Exposure (DLP) are the technologies in this category. Powder bed fusion has two subcategories, for polymers and metals but both operate similarly. Powder bed fusion occurs when powdered materials are fused when exposed to thermal energy. For polymers this process is called Selective Laser Sintering (SLS), for metals, the technologies include Direct Metal Laser Sintering (DMLS), Selective Laser Melting (SLM), and Electron Beam Melting (EBM). Material Jetting is simply the process of

selectively depositing material droplets and curing them. The two technologies for this process are called Material Jetting (MJ) and Drop On Demand (DOD). Binder Jetting is a similar process to material jetting but instead of depositing material, a liquid bonding agent is selectively deposited in a powder to create parts. This technology is simply called Binder Jetting (BJ) [23]. Each technology has its benefits, drawbacks, and applications. For example

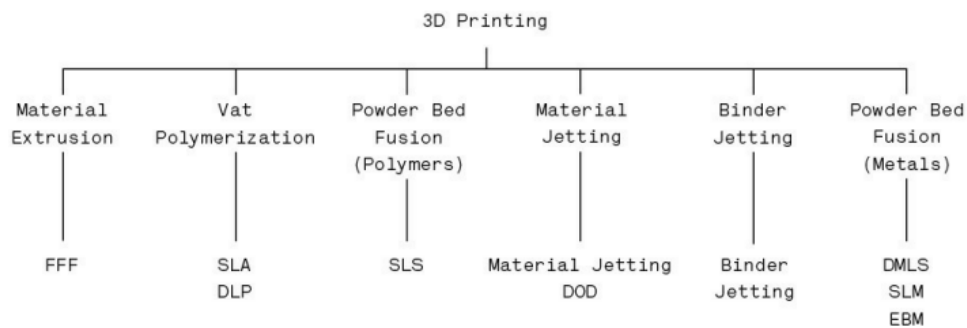


Figure 4: Additive Manufacturing Processes [23]

Additive manufacturing, or 3D printing as it is commonly referred to, allows for the fabrication of designs that would normally be impossible to manufacture with traditional methods. This increase in available designs has also led to an increase in available materials, specifically for FDM. Thermoplastic filaments like PLA and ABS are the most common materials used in FDM [24], but new engineering materials combined with additives such as fiberglass and carbon fiber are filling in the gaps of what FDM can be used for [25].

In contrast to subtractive manufacturing, AM creates three-dimensional objects by successively adding material, usually in a layer-by-layer method. Metal 3D printing is an ideal method for complex, low-quantity parts. Metal 3D printing has been used in aerospace, automotive, biomedical, personal protective equipment, and future Mars

exploration applications [26]. Specifically, the ability to print aluminum alloys known for their high strength-to-weight ratios combined with the high geometric control of AM has created a new degree of design optimization. [27] Layer-by-layer manufacturing allows designers to create complex open and closed cellular structures. Meaning that a closed cellular structure has cells that are completely enclosed and do not allow fluids to pass through them. The most common method for additively manufactured lattice structures is selective laser melting (SLM) a process that involves melting metallic powders to form highly dense structures with high accuracy [28]. Biomedical lattice structure implants manufactured from SLM have become increasingly popular in recent years. Creating implants that are close to the density of the bones are designed for ideal osseointegration. The aerospace industry has also found a use for AM lattice structures. Their lightweight properties can easily replace solid load-bearing objects. Even their thermal properties have been studied for applications in cooling channels for electronics on aircraft [29] [30].

2.4 Optimization

Many researchers have investigated the characteristics of heat sinks and how they can be optimized. Numerous variables can affect the performance of a heat sink. Increased fluid velocity, the thermal conductivity of the heat sink, and fluid medium, as well as physical geometry, are major factors in the performance of a heat sink. The surface area is a major sub-characteristic of the physical design of heat sinks. Newton's law of cooling states that heat transfer is directly proportional to the heat exchanger's surface area [11]. However other factors contribute to the total heat transfer in the system.

For example, orientation plays a significant role in a natural convection heat sink. This is due to the number of fins and the length of fins increasing the drag coefficient with an increasing angle of inclination. [31]. Carne developed an Artificial Neural Network (ANN) that generates a heat sink by adding material based on an equation that considers factors like velocity and convection rate [32].

Lattice structure applications are still being explored today and have yet to become commonplace in the industry despite their popularity in academic research. The structures' properties offer a promising base to be combined with other trending research areas for an even further optimized system. A catalyst-packed lattice structure was applied to a Fischer-Tropsch fixed bed reactor and significant improvements were realized due to the structures better conduction resulting in lower temperature gradients and improving performance [33]. Xusheng Hu used a periodic cellular structure in combination with a phase change material heat sink to improve thermal conduction through the heat sink. He conducted tests with lattice structures of different porosities and found that a phase change material heat sink with a lattice structure of 80% porosity showed the greatest enhancement ratio [34]. Porosity is a major parameter in most lattice heat exchanger optimization. Most porosities are around 70-90% but one study found that the operation time increases as porosity decreased. Meaning it takes longer to reach max temp for each power input [34]. Showing that the design of the heat sink largely depends on the application and requirements. Another study found optimal density was 20% for optimizing the Nusselt number for heat transfer [35].

Grading the lattice has shown to be another effective method of optimization or as post optimization improvement. A graded lattice has an inconsistent unit cell geometry, typically by increasing and or decreasing strut diameters by a linear factor at controlled points in one direction. Figure 5 shows an example of uniform, increasing, V-type, and W-type grading. Yun applied different patterns of grading lattice channels to improve the forced convection of the lattice heat exchanger [36]. He found the pressure drops and heat transfer through the simulation of four graded lattice structure channels as seen below. He also studied their thermo-fluid-structural performance by finding the von Mises equivalent stress in the structures as well. Yun found that the W-type grading had the lowest stress, the V-type had the highest pressure drop and the ungraded uniform channel had the best average heat transfer and lowest pressure drop.

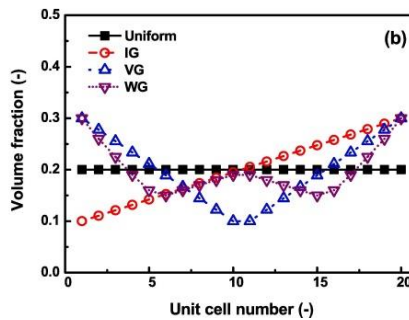
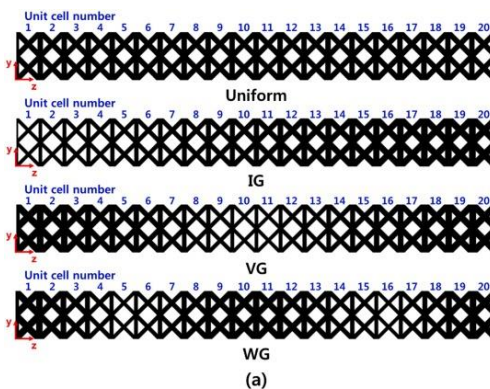


Figure 5: Yun's Graded lattice channel designs [36]

Due to the easily manipulable properties of lattice structures, integrating another intriguing geometry such as the honeycomb structure has been explored for improved heat transfer. One study explored the thermal performance of an X-lattice structure integrated with a honeycomb pattern as seen in Figure 6. The sandwich structure was tested in forced convection while being heated perpendicular to the flow. Increases friction factor and decreased turbulent kinetic energy. Heat transfer and pressure drop improved by 360% compared to the honeycomb structure and 40% to the X-lattice. T [37].

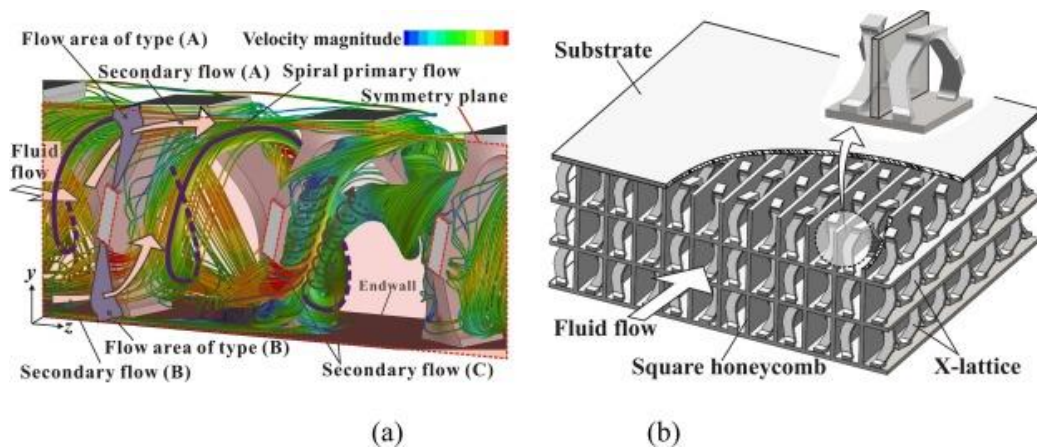


Figure 6: Yan's X-lattice Structure Integrated with a Honeycomb Structure [37]

Parametric optimization has also been performed on lattice structures. Vaissier optimized several cubical lattice structures by optimizing the ratio of the beam diameter of a strut to its cell size for an optimal surface-to-occupancy ratio. He then graded the heat sink linearly decreasing from the top to the bottom [38]. A limitation noted in his study is that the tradeoff made for optimal surface-to-occupancy ratio is lost after

grading. He then applied his optimization method to an industrial oil tank carter and industrial bent pipe. His method saw significant cooling for both applications verifying his method. The grading effect can be seen in Figure 7 between structures (c) and (d).

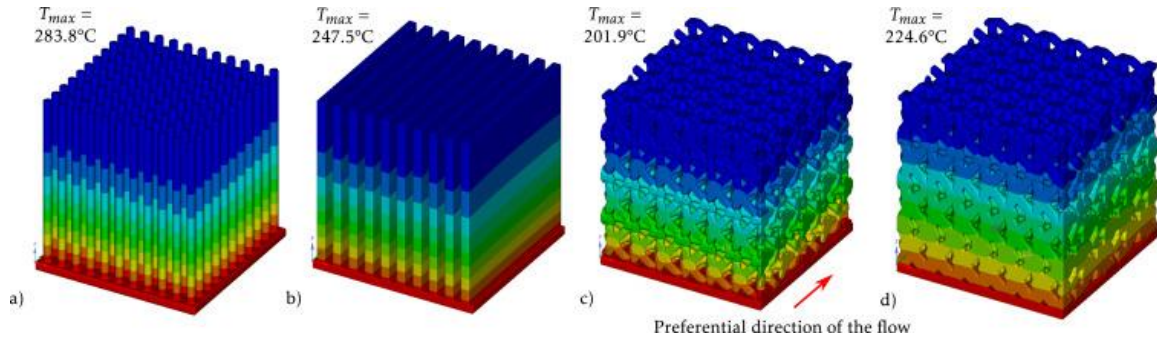


Figure 7: Heat Sinks from Vaissier's Study [38]

The commercially available software Design Expert has been used as a numerical simulation tool for optimization by other researchers [39] and even in additive manufacturing applications [40] [41]. It allows data to be quickly interpreted and visualized and then optimized using statistical models to predict outputs. This cuts down on creating physical experiments and the cost of materials. The software uses an analysis of variables (ANOVA) also called the Fisher analysis of variance, a statistical method that identifies the relationship between independent and dependent variables. It does so by identifying systemic variables and random variables. Systemic variables are the input parameters that influence the response values while random variables do not [42]. This method was originally employed for psychology studies but was later applied to a variety of research applications. This methodology allows for easy identification of parameters for optimization.

CHAPTER III

DESIGN OF EXPERIMENTS

3.1 Introduction

For our experiments, certain constraints were set to narrow the scope of our work. The heat transfer conditions were set to accurately reflect the conditions of small electronics heat sinks. This means that natural convection or passive cooling is the method of heat transfer. Other studies have done similar heat transfer models with lattice structure heat sinks but only considered conduction through the heat sink, which is significantly more computationally friendly and only accurate for low fluid density scenarios such as high-altitude applications. For our purposes, internal conduction was only visually evaluated, however, the maximum and minimum temperatures of the lattice structure were monitored which approximately shows the structure's capabilities of distributing heat.

A design of experiments was used for this study. This allowed for a significantly reduced time for modeling and analyzing the results. Design Expert 10, the design of experiments software allows the user to select inputs and identify their relationship with selected outputs. This software has been used by other published works and this study follows a similar methodology. Research began by identifying mutable lattice structure parameters and the responses that characterized heat sinks. Unit cell geometries were

selected to be easily fabricated with FDM technologies. Once the initial parameters of the research were decided upon, the Design of Experiments was created. This model requests the responses of specific lattice structure heat sinks to build the numerical optimization model. The data was collected using multiple CFD simulations. The data was entered into the model and analyzed to identify a few optimized structures. The structures were then created in 3D CAD and run through the CFD simulation to validate the accuracy of the model. The final step of this research would be to experimentally test the 3D-printed heat sinks to determine the percent error of our methodology.

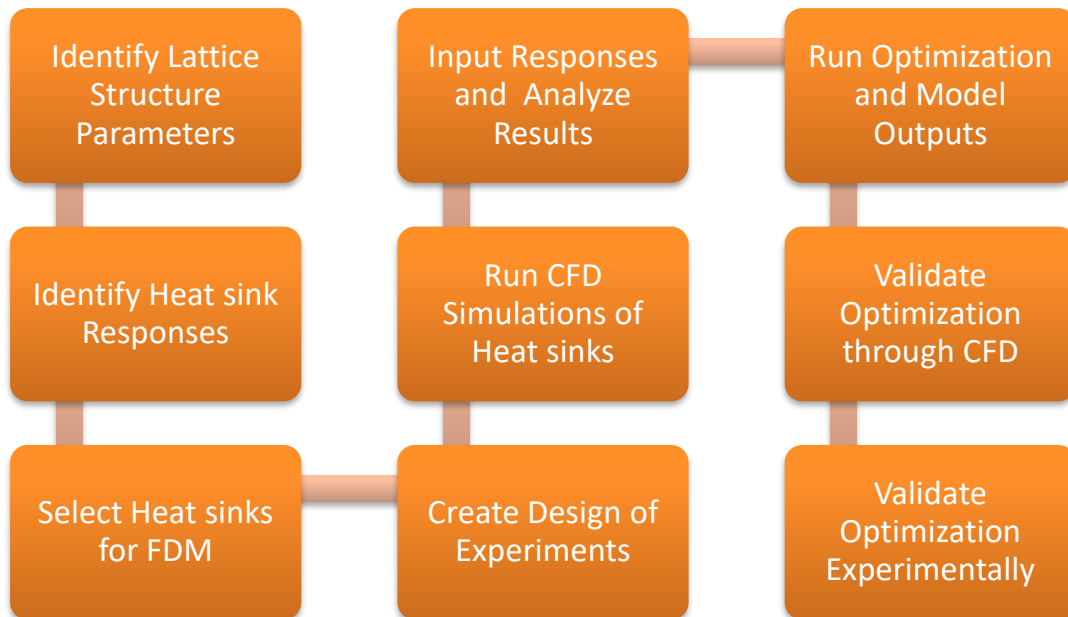


Figure 8: Research Methodology Flowchart

3.2 Selection of Parameters and Modeling

For our study, the inputs were chosen from the manipulatable geometric features of lattice structures. The modeling software Netfabb by Autodesk was used to model the lattice structures using the comprehensible “Lattice Commander” tool. This tool allows the modeler to transform bodies into a volume lattice structure. While some other features were available the chosen alterable parameters of the lattice structure were strut diameter, unit cell size, and unit cell type. Where the strut diameter is defined as the diameter of the cross-section of the struts of the lattice and the unit cell size is the length of one of the repeated cells that makes up the 3D lattice array.

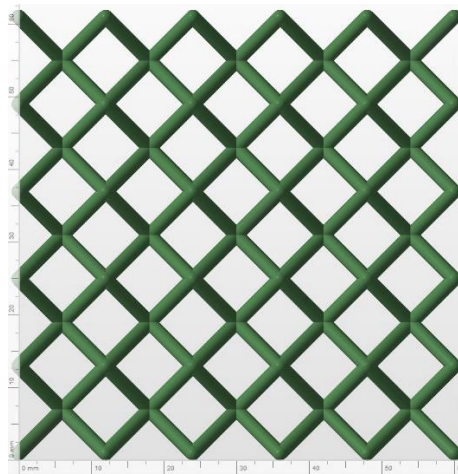


Figure 9: Side View of 'X' Lattice Structure

The outputs for the design of the experiment were chosen as those that can be used to evaluate heat sinks. The most significant of those being heat transfer (W) This value shows how much energy, in watts, the heat sink removes from its footprint area. Related to heat transfer is the heat transfer coefficient. This value shows the energy removed from the footprint per degree Kelvin. Another output selected was thermal resistance, which shows the resistance of heat flow through an area. The final output for

our design of experiments was surface area. Based on the basic equation for convection heat transfer, the surface area is positively associated with increased convection heat transfer, therefore increasing it theoretically should increase heat transfer since it is the main method of heat transfer for natural convection heat sinks. Table 1 shows the design of the experiments table along with the selected ranges for the inputs.

Table 1: Design of Experiments Parameters

Lattice Structure Variable	Range of Optimization	Heat Transfer (W)	Heat Transfer Coefficient (W/m ² -K)	Thermal Resistance (K/W)	Surface Area (m ²)
Strut Diameter	2mm, 4mm, 6mm, 8mm				
Cell Size	10mm, 12mm, 15mm, 20mm				
Cell Type	X, W, Soft Box, Dark Horse, Icosa, Crush				

The minimum strut diameter was selected as 2mm since this is the recommended feature size for FDM printers. 8mm was selected as the maximum value since most lattice structures became closed-cell structures at or past this value. The volume of the cube used to create the volumetric lattice was chosen as 60mm x 60mm x 60mm, this is a typical size seen on small electronics or computers. Given a 60mm cube, cell sizes were chosen as 10mm, 12mm, 15mm, and 20mm effectively creating 6, 5, 4, and 3 unit cells along a coordinate. Netfabb offers 25 unit cell types. To narrow the scope of this study 6 were chosen based on a manufacturability evaluation for FDM. Primarily, if the lattice would need support structure while printing. After creating the design of experiments the software creates a list of lattice structures with varying combinations of the input parameters.

It should be noted that the Cell type was chosen as a nominal categorical parameter, which is used for cases of different classifications or “types” when computing the optimization. The following table shows the generated list of lattice structures to be created for the data-based design of experiments. The feature, “Categoric Balance’ was also selected for this study. This creates an equal number of lattices (3) for each structure. Table 2 shows what Design Expert requested to build the model.

Table 2: Requested Lattice Structures from the DOE

Run	Factor 1: Strut Diameter	Factor 2: Cell Size	Factor 3: Unit Cell Type
1	6	15	W
2	2	10	Icosa.
3	8	20	Icosa.
4	6	10	Soft Box
5	6	15	X
6	4	10	Dark Horse
7	2	20	Dark Horse
8	8	15	Crush
9	8	10	Dark Horse
10	8	20	Icosa.
11	4	15	Crush
12	4	15	Soft Box
13	4	15	Soft Box
14	6	15	X
15	6	15	W
16	4	15	Crush
17	8	10	X
18	2	15	W

The computational fluid dynamics (CFD) simulations were all completed in Star CCM+ [43]. The conditions of the simulation were set up so that they accurately reflected that of the operation of a heat sink. A constant temperature of 375 degrees kelvin was

applied to the base of the heat sink and the energy leaving the heat sink was monitored. All simulations were run until they were in a steady state.

Once the simulations were completed the output data was entered into Design Expert. After the initial 18 lattice structure heat sinks from the design of experiments were run in a CFD simulation, the results were initially analyzed to identify trends. For the optimization process three optimizations were run, each narrowing in on key parameters and trends. found. The final optimization yielded three optimized lattices. These lattices were modeled in Netfabb and ran through the same CFD simulation that the original 18 heat sinks were to validate the results of the optimization. Results from the simulation were then compared to the optimization.

3.3 Design of Experiments

After reviewing the initial lattice structure heat sinks simulation data, immediate trends were found. The best-performing heat sink from the DOE had a strut diameter of 2mm and a cell size of 15mm. The simpler lattice structures “W” “Soft Box” and “X” cell types had the best heat transfer results, with “W” performing the best. The Heat transfer coefficient results were similar as expected. The 2mm strut diameter and the 15 mm cell-sized lattice along with the “W”, “Soft Box” and “X” Cell types performed the best as well. The Thermal resistance output best-performing lattice was a 2mm strut diameter and 15mm cell size. However, the “W” and “X” unit cell types distinguished themselves in this output, having the lowest thermal resistances. The largest surface area came from a 2mm strut diameter and a 10mm cell-sized lattice. While all lattices were relatively similar in surface area the “X” cell type had a noticeably larger surface area

than the rest of the unit cells. Table 3 shows all 18 lattice structure heat sinks and their outputs from the CFD simulation.

Table 3: Results from DOE Simulations

Run	Factor 1: Strut Diameter	Factor 2: Cell Size	Factor 3: Unit Cell Type	Response 1: Heat Transfer (W)	Response 2: Heat Transfer Coefficient (W/m ² *K)	Response 3: Thermal Resistance (K/W)	Response 4: Surface Area (m ²)
1	6	15	W	11.170	2.397	6.713	0.062
2	2	10	Icosa	9.290	1.103	8.069	0.112
3	8	20	Icosa	6.060	3.116	12.700	0.025
4	6	10	Soft Box	3.100	2.089	19.100	0.025
5	6	15	X	11.790	2.565	6.356	0.061
6	4	10	Dark Horse	7.696	1.253	9.740	0.082
7	2	20	Dark Horse	3.520	2.127	21.300	0.022
8	8	15	Crush	3.350	2.453	22.400	0.019
9	8	10	Dark Horse	3.550	1.775	21.100	0.027
10	8	20	Icosa	6.060	3.116	12.700	0.025
11	4	15	Crush	5.910	0.954	12.700	0.083
12	4	15	Soft Box	16.410	3.698	4.568	0.059
13	4	15	Soft Box	16.410	3.698	4.568	0.059
14	6	15	X	11.790	2.565	6.356	0.061
15	6	15	W	11.170	2.397	6.713	0.062
16	4	15	Crush	5.910	0.954	12.700	0.083
17	8	10	X	3.670	2.247	15.500	0.287
18	2	15	W	19.860	6.510	3.776	0.041

CHAPTER IV

OPTIMIZATION AND DISCUSSION

4.1 Optimization Methodology

Design Expert's optimization function was used to conduct 3 numerical optimizations. Each optimization's criteria were refined with the first being "lightly constrained" the second being "moderately constrained" and the third being "heavily constrained." These optimizations were concluded and adequately refined based on the number and quality of the results produced. For example, Optimization #1 should yield several results that allow the user to identify general trends of the study and make a considerable refinement to the parameters and importance ratings that will be discussed later. The second optimization's goal was to be able to identify the key parameters and ranges that influence the performance of the heat sinks. Optimization #3's objective was to narrow in on the ideal range of key parameters and find important factors so that a few results are produced.

Design Expert's numerical optimization can optimize for multiple goals of varying importance as selected by the user. Input parameters and responses can be set to goals of maximize, minimize, target, in range, or equal to. Limits to each value range can also be set for each goal. For this study, heat transfer, heat transfer coefficient, and surface areas were set to maximize, and thermal resistance was set to minimize for every

optimization. In addition, to goals, the “importance” can be set for each response of the optimization. Each response is selected by the user from a range of “+” meaning lowest importance to “++++” representing critical importance. An importance rating of “+++” is considered moderately important and is the default rating for a response. The importance of the responses was a crucial part of the optimization since the responses used for the evaluation of the heat sink were selected to evaluate the heat sink from a theoretical standpoint. Since heat transfer was the only truly important response of the heat sink, it was treated as such and set at the maximum importance (++++) for each optimization.

4.2 Optimization Process

Optimization #1 was run with very little refinement from the initial set of parameters. The strut diameter was the only input that was refined for this optimization. The range was narrowed from 2mm to 8mm to 2mm to 6mm. This was because structures with 8mm struts generally had the worst heat transfer with the best-performing heat sink having a heat transfer of just over 6 W. Importance values for this run were selected based on the initial assumptions about the importance of each output, with heat transfer being the highest level of importance for this and all optimizations. The heat transfer coefficient is closely related to heat transfer and was selected as “++++”. Thermal resistance and surface areas were kept at the initial moderate importance (+++). Table 4 shows inputs for optimization #1.

Table 4: Optimization #1 Criteria

Geometric Parameter	Goal	Response Parameter	Goal & Importance
Strut Diameter	In Range: 2mm to 6mm	Heat Transfer	Maximize, +++++
Cell Size	In Range: 10mm to 20mm	Heat Transfer C.	Maximize, +++++
Cell Type	In Range: All	Thermal Resistance	Minimize, +++
-	-	Surface Area	Maximize, +++

The desirability output seen in the last column is a value that ranges from 0 to 1. While numerical optimization finds a combination of parameters that maximizes this value, the user's goal is not to try to maximize this value. This value represents how closely the upper and lower limits are set relative to the actual optimum value. The numerical optimization is designed to meet the goals and return the highest desirable solutions for the criteria set. For our final optimization, the highest desirability we received was 0.826.

Table 5: Results from Optimization #1

Number	Strut Diameter	Cell Size	Unit Cell Type	Heat Transfer	Heat Transfer Coefficient	Thermal Resistance	Surface Area	Desirability
1	2.000	16.608	W	17.266	4.079	2.155	0.050	0.811
2	2.000	20.000	X	15.511	3.556	2.937	0.095	0.739
3	2.054	20.000	X	15.453	3.555	3.008	0.094	0.738
4	2.000	19.820	X	15.473	3.531	2.946	0.096	0.736

5	2.000	19.599	X	15.425	3.499	2.958	0.098	0.733
6	2.370	20.000	X	15.115	3.545	3.422	0.093	0.730
7	2.000	14.107	Soft Box	14.993	3.352	5.877	0.050	0.696
8	2.000	14.057	Soft Box	14.982	3.345	5.880	0.050	0.695
9	2.000	18.707	Icosa	11.855	2.858	5.808	0.050	0.591
10	2.000	18.539	Icosa	11.819	2.834	5.817	0.051	0.589
11	2.000	17.627	Crush	9.189	1.931	11.427	0.050	0.404
12	2.000	17.774	Crush	9.220	1.952	11.419	0.049	0.403
13	2.000	17.883	Crush	9.243	1.968	11.414	0.048	0.403
14	2.000	17.985	Crush	9.266	1.983	11.408	0.047	0.403
15	2.000	18.113	Crush	9.293	2.001	11.401	0.046	0.402
16	2.000	18.163	Crush	9.304	2.008	11.399	0.045	0.402
17	2.000	13.773	Dark Horse	7.870	1.862	13.863	0.049	0.344
18	2.000	13.812	Dark Horse	7.878	1.867	13.861	0.048	0.344
19	2.000	13.722	Dark Horse	7.859	1.854	13.866	0.049	0.344
20	2.000	13.684	Dark Horse	7.850	1.849	13.868	0.049	0.344
21	2.000	13.872	Dark Horse	7.891	1.876	13.858	0.048	0.344
22	2.000	13.940	Dark Horse	7.905	1.886	13.854	0.047	0.344
23	2.000	13.975	Dark Horse	7.913	1.891	13.853	0.047	0.344
24	2.000	14.024	Dark Horse	7.924	1.898	13.850	0.046	0.344
25	2.000	14.712	Dark Horse	8.072	1.996	13.813	0.041	0.340

The outputs from optimization #1 are shown in Table 5. From the criteria set, 22 solutions were found with desirability ranging from 0.811 to 0.344. This optimization yielded at least one result for each unit cell type, although it can quickly be determined that the best-performing heat sinks were the “W” and “X” cell types. A maximum heat transfer from this optimization was found at 17.266W. The most notable outcome from

this optimization was the strut diameter values. Of the 22 structures produced, 20 of 22 had a strut diameter of 2mm. As mentioned previously in this paper, 2mm was set as the minimum strut diameter based on FDM design constraints, however, if other technologies were used this could suggest that the ideal strut diameter could be less than 2mm. The only 2 solutions that did not have a strut diameter of 2mm were “X” cell-type structures.

Given the information found from optimization #1, the next optimization was set up to target these trends and enable optimization #3 to yield a few optimized heat sinks. For optimization #2, strut diameter and cell size were refined, and importance values were altered to allow for better heat transfer results. The strut diameter range was greatly reduced from 2mm to 6mm to 2mm to 3mm. The cell size range was also slightly reduced from 13mm to 20mm. All cell types were left available as solutions for this trial to confirm results from the first optimization. The importance values for heat transfer coefficient were changed from “++++” to “+++” and thermal resistance and surface area were both changed from “+++” to “++”. These changes were made to increase and allow the optimization to focus more on creating solutions with better heat transfer. Table 6 shows inputs for optimization #2.

Table 6: Optimization #2 Criteria

Geometric Parameter	Goal	Response Parameter	Goal & Importance
Strut Diameter	In Range: 2mm to 3mm	Heat Transfer	Maximize, +++++
Cell Size	In Range: 13mm to 20mm	Heat Transfer C.	Maximize, +++
Cell Type	In Range: All	Thermal Resistance	Minimize, ++
-	-	Surface Area	Maximize, ++

Table 7: Results from Optimization #2

Number	Strut Diameter	Cell Size	Unit Cell Type	Heat Transfer	Heat Transfer Coefficient	Thermal Resistance	Surface Area	Desirability
1	2.000	16.608	W	17.266	4.079	2.155	0.050	0.745
2	2.000	20.000	X	15.511	3.556	2.937	0.095	0.633
3	2.000	19.936	X	15.498	3.547	2.940	0.095	0.632
4	2.000	19.818	X	15.472	3.530	2.946	0.096	0.629
5	2.190	20.000	X	15.308	3.551	3.185	0.094	0.624
6	2.605	20.000	X	14.864	3.538	3.730	0.093	0.602
7	2.000	14.107	Soft Box	14.993	3.352	5.877	0.050	0.584
8	2.000	14.387	Soft Box	15.053	3.393	5.862	0.048	0.582
9	2.000	19.785	Icosa	12.088	3.012	5.751	0.041	0.377
10	2.000	19.850	Icosa	12.101	3.022	5.747	0.040	0.377
11	2.000	19.719	Icosa	12.073	3.003	5.754	0.041	0.377
12	2.000	19.652	Icosa	12.059	2.993	5.758	0.042	0.377
13	2.000	19.967	Icosa	12.127	3.039	5.741	0.039	0.377
14	2.000	19.564	Icosa	12.040	2.981	5.762	0.043	0.377
15	2.000	19.434	Icosa	12.012	2.962	5.769	0.044	0.376
16	2.000	19.259	Icosa	11.974	2.937	5.779	0.045	0.376
17	2.000	18.988	Icosa	11.916	2.898	5.793	0.048	0.374

From optimization #2, 14 solutions were found with desirability ranging from 0.745 to 0.376. Outputs from this optimization are shown in Table 7. This optimization found at least one solution for the W, X, Soft Box, and Icosa structures, notably excluding Crush and Dark Horse. Again, the W and X lattice structures had the highest heat transfer results. The optimization found the same W-type lattice structure from the

previous optimization as the best solution again with a heat transfer of 17.266 W. From the results, it can be seen that the heat transfer coefficient was generally proportional to the heat transfer and was a good indicator of heat transfer. The thermal resistance was also generally inversely proportional to the heat transfer; however, it varied significantly based on unit cell type. The surface area surprisingly had little correlation to the heat transfer values. For example, solution #1 had a surface area of 0.05 m² and solution #2 had a surface area of 0.095 m², nearly twice as large of a surface area. Their corresponding heat transfer values represent the opposite logic to the theoretical strategy of maximizing surface area for increased convection heat transfer.

Optimization #3 was highly constrained using the trends and results gathered from the previous optimizations. Table 8 shows the parameters used for the final optimization. The strut diameter was changed from an “in range” goal to a “target” of 2 mm with limits of 2 mm to 3 mm. Importance was also set on this input parameter of “+++++”. As the previous optimizations showed, 2 mm was the ideal diameter available for heat transfer and was the most significant parameter found from the first two optimizations. Adding the critical importance factor also allowed for fewer solutions to be found than leaving the moderate importance. The cell size was left at the previous range of 13 mm to 20 mm since no clear trends were identified in this category, but all solutions found values within this range. The cell type was set to be equal to W. In all optimizations and of the 18 lattice structure heat sinks from the design of experiments, the W structure had the highest heat transfer values. The importance values were left the same from optimization #2 for all responses. Table 8 shows inputs for optimization #3.

Table 8: Optimization #3 Criteria

Geometric Parameter	Goal	Response Parameter	Goal & Importance
Strut Diameter	Target: 2mm, From 2mm to 3mm, +++++	Heat Transfer	Maximize, +++++
Cell Size	In Range: 13mm to 20mm	Heat Transfer C.	Maximize, +++
Cell Type	Equal to 'W'	Thermal Resistance	Minimize, ++
-	-	Surface Area	Maximize, ++

Table 9: Results from Optimization #3

Number	Strut Diameter	Cell Size	Unit Cell Type	Heat Transfer	Heat Transfer Coefficient	Thermal Resistance	Surface Area	Desirability
1	2	16.608	W	17.226	4.079	2.155	0.05	0.826
2	2	15.771	W	17.086	3.959	2.2	0.057	0.814
3	2	18.404	W	17.652	4.337	2.06	0.035	0.783

From the results of optimization #3, 3 solutions were found. Table 9 shows the numerical solutions. With the higher importance being placed on the strut diameter, all solutions had a strut diameter of 2 mm. Since the cell type was set to the W cell type, the only parameter that varied was the cell size. The three cell sizes varied from 15.771 mm, 16.608 mm, and 18.404 mm. As mentioned in the methodology section of this text, the initial cell sizes were set so that the total number of cells would be an integer value, so that no cells were partially constructed. From our optimization, the cell sizes generated

do not create completed cells. The effects of this are unknown and should be further investigated.

As seen from the optimization, the maximum heat transfer structure is a different structure generated than the best-performing structure in the previous two optimizations. With the new structure having a heat transfer of 17.652 W. The heat transfer and heat transfer coefficient appears to be inversely proportional to the cell size from the three structures generated. From the thermal resistance results, it can be found that the resistance decreases as heat transfer increases this follows theoretical logic and shows that the thermal resistance of the structure could be a good indicator of heat transfer for lattice structures. The surface area results were surprisingly inversely proportional to the heat transfer of the lattice structure. This goes against any simple hypotheses that increasing the surface area of a lattice structure could be a method of optimization for lattice structures. This shows that lattice structures are more complex than those having a high surface area to volume ratio and that the geometry of the structures plays an important role in heat transfer.

4.3 Validation

Once these structures were generated in Netfabb with the exact criteria specified from the design of experiments, they were converted to STLs for validation. It was found that these lattices needed additional surface repair to mesh. In Netfabb, a surface repair script, 3 mm blending, and 2% smoothing were found to be sufficient to import the parts with no errors. The main reason for all these repairs was surface quality issues around the nodes. The blending alone created divots in the top and bottom of the nodes which

created an unacceptable number of cells for each node. Instead of setting up specific controls for every node on each part, the model was repaired so that it could mesh without excessive controls. It is unclear why these models required additional processing to import them into Star CCM+. The changes made in the topology likely affected the performance of the heat sinks, but it is unclear to what extent. The following figures display the three optimized lattices after surface repairs were made.

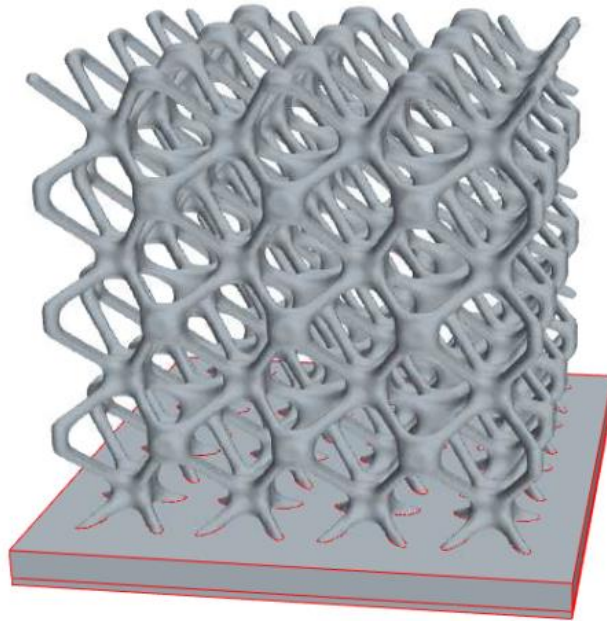


Figure 10: Optimized Lattice Structure #1: Cell Size of 15.771 mm [43]

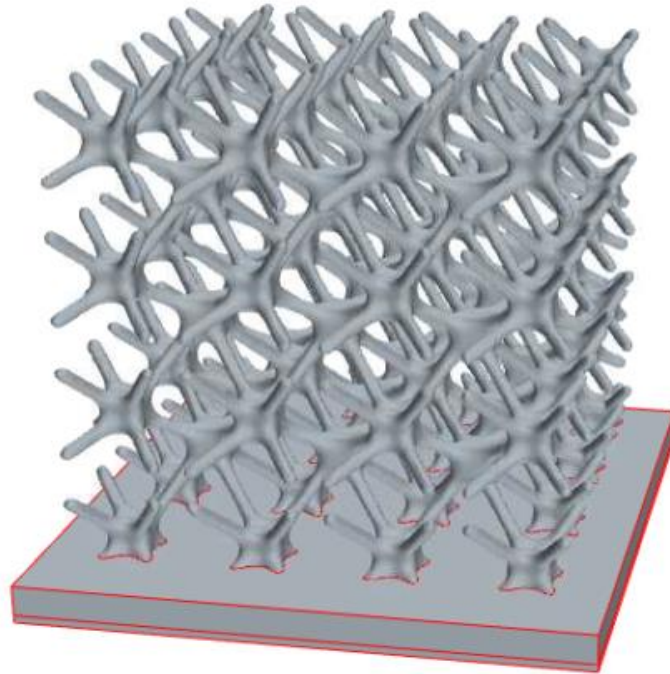


Figure 11: Optimized Lattice Structure #2 Cell Size of 16.608 mm [43]

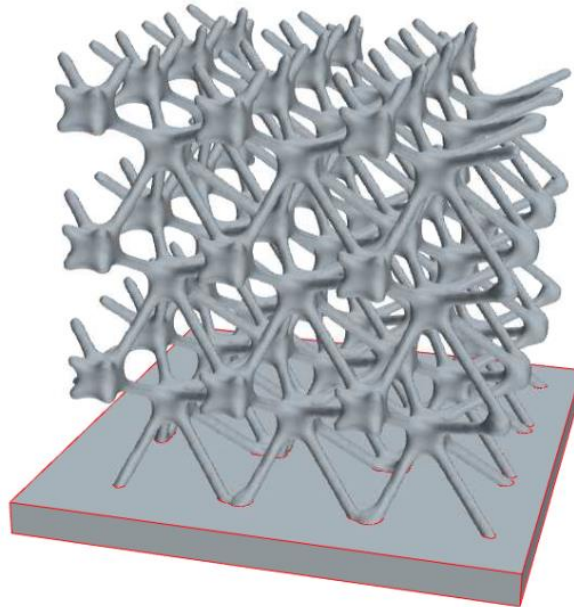


Figure 12: Optimized Lattice Structure #3 Cell Size of 18.404 mm [43]

The outputs from the CFD simulation included the same ones from the design of experiments: heat transfer, heat transfer coefficient, and thermal resistance. In addition,

the maximum and minimum temperature of the fin surface was added as an additional metric between the heat sinks. The results from the three simulations are in Table 10.

Table 10: CFD Results of Optimized Heat Sinks

	Heat Transfer (W)	Heart Transfer Coefficient of Heat Transfer ($W/m^2 \cdot K$)	Thermal Resistance (K/W)	Max Temp (K)	Min Temp(K)
Opt. #1	26.8	10.9	1.5	374.951	334.954
Opt. #2	22.7	7.7	2.1	374.97	327.305
Opt. #3	19.9	7.0	2.3	374.734	328.457

From the results of the CFD, we can see the optimized structures overperformed significantly in heat transfer and heat transfer coefficient. From the optimization software, we expected results around 17.0 to 17.6 W. While it is encouraging that the results were better than expected, this difference could indicate that the numerical optimization methodology may need a larger sample size to train the ANOVA model. To determine whether the difference was from the optimization not having enough data to find accurately predict performance or from the errors in CFD modeling, experimental testing will be performed. This work is still underway due to lead times for receiving the heat sinks.

Table 11: Percent Difference Between DOE and CFD

	% Difference HT	% Difference HTC	% Difference TR
Opt. #1	36.25	63.68	46.67
Opt. #2	24.11	47.03	2.62
Opt. #3	11.30	38.04	10.43

CHAPTER V

MANUFACTURING

5.1 Introduction

For experimental testing of the lattice structures, many methods of manufacturing were explored. Lattice structures would be impossible to fabricate with traditional methods of manufacturing like extrusion, stamping, casting, or machining. As mentioned in the literature review chapter, selective laser sintering (SLS) is a commonly employed additive manufacturing method for fabricating lattice structure heat sinks. While new materials are being developed for SLS printers, there is a known obstacle when working with copper powders. Since copper has a very high thermal conductivity the heat from the sintered part spreads through the powder fusing nearby particles. This leads to dimensionally inaccurate parts. For this reason, aluminum is a much stronger candidate for this additive manufacturing method. SLS printing is typically a more expensive method but is capable of fabricating parts without a support structure where an FDM printer would need support. However, FDM printers still can create parts beyond what traditional methods can produce. This is largely accredited to the layer-by-layer nature of manufacturing that allows for internal features in designs.

As per the scope of this research, test samples were manufactured using a low-cost FDM printer. Using a copper and polylactic acid (PLA) blended filament, we were

able to produce mostly copper structures following a de-binding and sintering post-processing. A Creality Ender 5 was used to print all parts of this research. The printer was slightly upgraded with an all-metal direct drive extruder and hardened steel nozzles. These upgrades were both recommended by the filament manufacturer for this printer. A metal hot end is required when working with this material to protect the printer from damage. Though the printer's original heating element can reach these temperatures, instances of heat creep can damage some of the plastic components on the printer. The hardened steel nozzle was required due to the abrasiveness of the copper in the filament. Standard brass nozzles wear out quickly when working with filaments with hard additives and this is a commonly reported issue. Both components cost less than \$100 and required very little technical experience working on 3D printers to install.

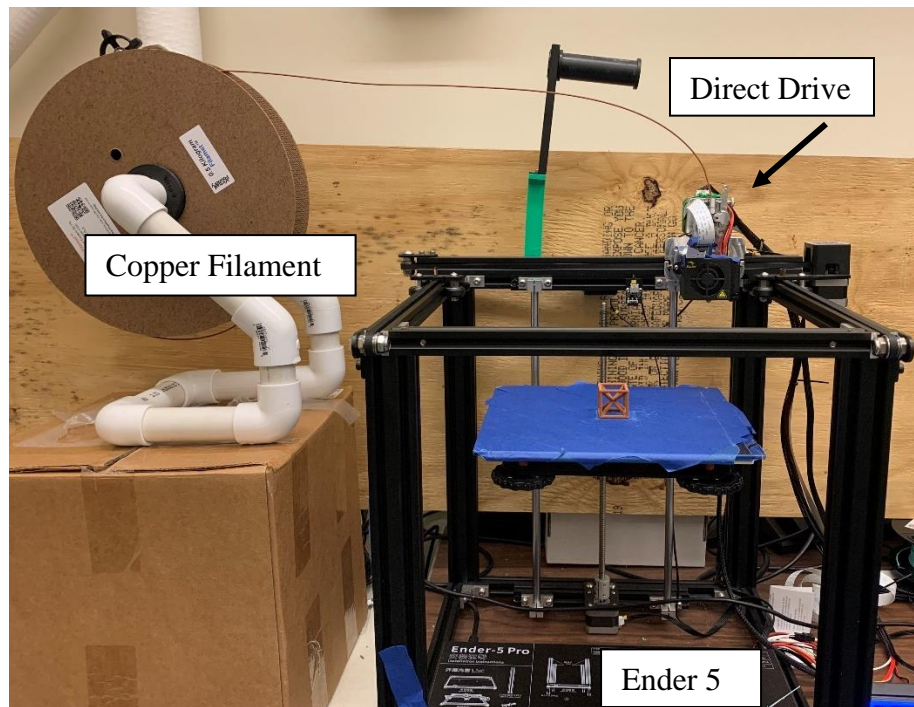


Figure 13: 3D Printer Setup

The copper-infused filament used in this study was purchased from The Virtual Foundry. The manufacturing methodology used in this study comes from their website except for some specific 3D printing settings that we found worked best on our printer. Table 12 shows some of the specific settings we found contributed to improved print quality. Some of these settings we believe are specific to our printing setup. For example, the retraction settings were finely tuned after the addition of the direct drive extruder that was purchased for this printer. Most settings can be left unchanged from a PLA configuration. However, to produce “100%” copper parts, the infill percentage was set to 100% so that there were no voids in the part.

Table 12: 3D Printer Settings for Copper Filament

	Extruder Temp	Bed Temp	Fan Speed	Flow %	Retraction Speed	Retraction Distance
Value	225 °C	50 °C	0	135 mm/s	32 mm/s	3.5 mm

Once the copper parts have been printed, there is a two-part heat treatment required to yield the mostly copper parts. The first step is the “Debind” process. This is the term Virtual Foundry defines this as the process that removes the binder material and leaves behind a porous metal structure. The second step, sintering, bonds the metal particles together, increasing density and strength. These two processes can be accomplished in a kiln following the sintering temperatures and time seen in Figure 16.

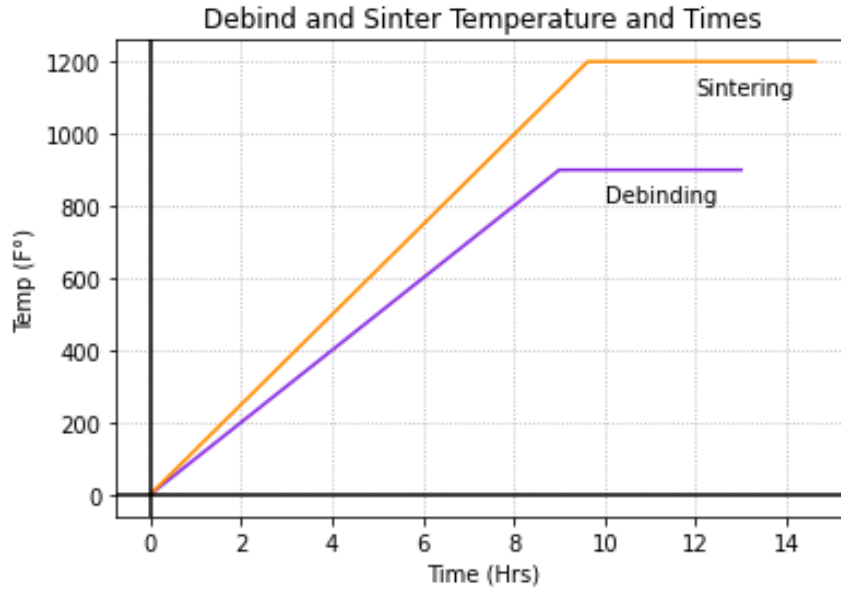


Figure 14: Copper Debind and Sintering Temperature and Times [44]

For the debinding process, parts should be suspended in Al_2O_3 refractory in a crucible and tamped from the top to pack the parts in. The crucible with the parts should be placed in the kiln and ramped at $100^\circ F$ and hour to $900^\circ F$. Hold the temperature at $900^\circ F$ for 4 hours and let the furnace return to room temperature. For the sintering process, suspend the part in the talc refractory, leaving at least 25mm of room at the top of the crucible. Tamp the sides so that the talc has settled around the part. Fill up the 25mm of space in the crucible with sintering carbon. Place the crucible with the parts in the kiln and ramp at $200^\circ F$ an hour to $1925^\circ F$ and hold for 5 hours. Once the furnace has returned to room temperature remove the parts and use a wire brush to clean the parts. These temperatures and times may vary on the size of the part but require experimentation to optimize this process.

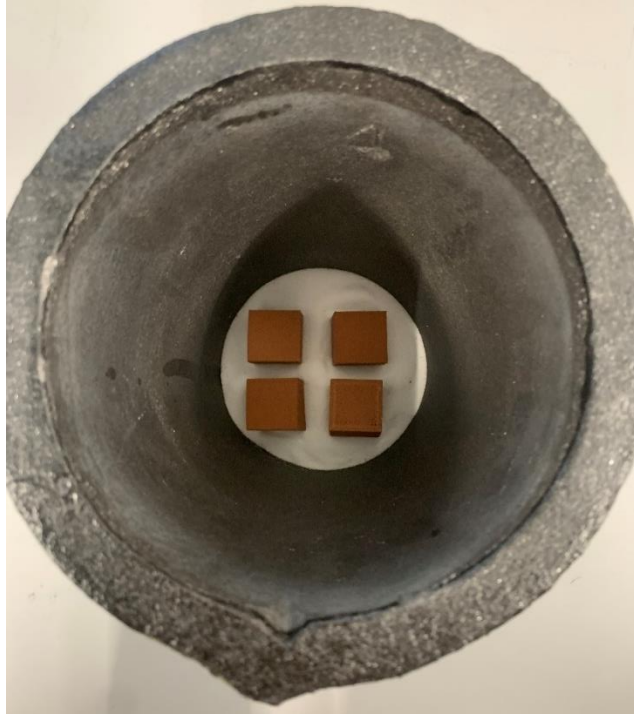


Figure 15: Copper Samples in Crucible Before Debinding



Figure 16: Copper Parts in Crucible in Furnace



Figure 17: Copper Samples Buried in Talc and Sintering Carbon

5.2 Shrinkage Study

It is known that the process of debinding the part causes a significant amount of shrinking of the part. To account for this a shrinkage study was performed to determine the net change of the part after the debind and sintering processes. This study is important to create dimensionally accurate final parts. Keeping in mind the 4 elements for characterization of the study, performance, modeling, design, and manufacturing, this is an excellent example of the interconnectedness of these elements. Our modeling determines the size of the final part to produce but given our manufacturing method, our design needs to change to achieve the same performance we expect. To accomplish this 10mm cubes were used to measure the shrinkage along the x y and z directions. The image below shows what the printed, debinded, and sintered (polished) cubes look like. The shrinkage is visible between the printed and sintered cube. While shrinkage occurs between the printed and debinded stages, only the final shrinkage is needed for our study.

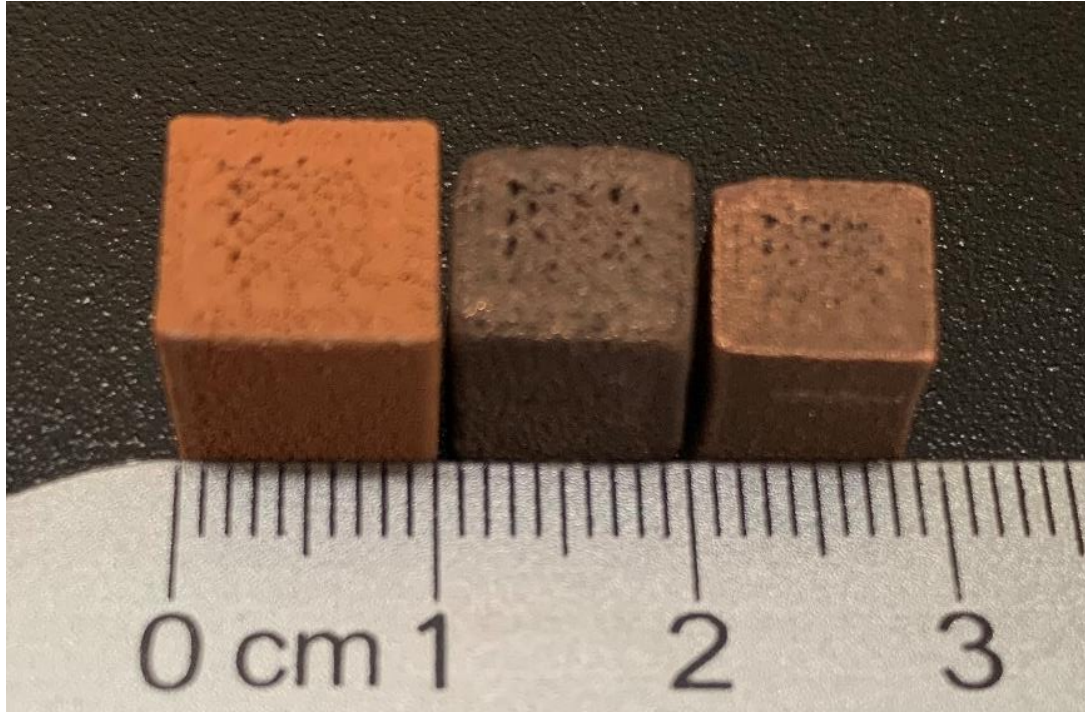


Figure 18: Printed, Debinded, and Sintered Copper Samples

As seen from the picture, the sintered parts experienced some warping and came out with an hourglass figure. This was accounted for in our shrinkage study by measuring at various heights, so this effect was averaged in the analysis. More experience with sintering the parts should eliminate this effect. Two sintered parts and two printed parts were used as the samples for this study. Tables 13 and 14 show the shrinkage study's results and shrinkage ratio.

Table 13: Shrinkage Study Measurements

Part	dim.	Measurement 1 (in)	Measurement 2 (in)	Measurement 3 (in)	Measurement 4 (in)	Measurement 5 (in)	Average (in)	Average Dim
Sintered 1	x	0.361	0.365	0.356	0.359	0.364	0.361	0.344
	y	0.360	0.362	0.359	0.365	0.363	0.3618	0.343
	z	0.382	0.381	0.382	0.383	0.382	0.382	0.363
Sintered 2	x	0.321	0.334	0.324	0.334	0.322	0.327	-
	y	0.319	0.326	0.320	0.326	0.330	0.3242	-
	z	0.344	0.343	0.346	0.343	0.346	0.3444	-
Printed 1	x	0.396	0.403	0.397	0.397	0.402	0.399	0.399
	y	0.397	0.402	0.398	0.396	0.397	0.398	0.398
	z	0.397	0.398	0.397	0.397	0.397	0.3972	0.398
Printed 2	x	0.399	0.401	0.400	0.397	0.398	0.399	-
	y	0.397	0.402	0.398	0.397	0.396	0.398	-
	z	0.400	0.397	0.398	0.398	0.399	0.3984	-

Table 14: Final Shrinkage Ratios

Dim.	Shrinkage Ratio
X	13.78
Y	13.82
Z	8.70

Interestingly, we see that the x and y dimensions had very similar ratios while the z direction experienced about 5% less shrinkage. Most slicing software allows for anisotropic scaling of parts by percentage. Creating dimensionally accurate final parts is as simple as scaling the x, y, and z dimensions by 13.78%, 13.82%, and 8.7% respectively.

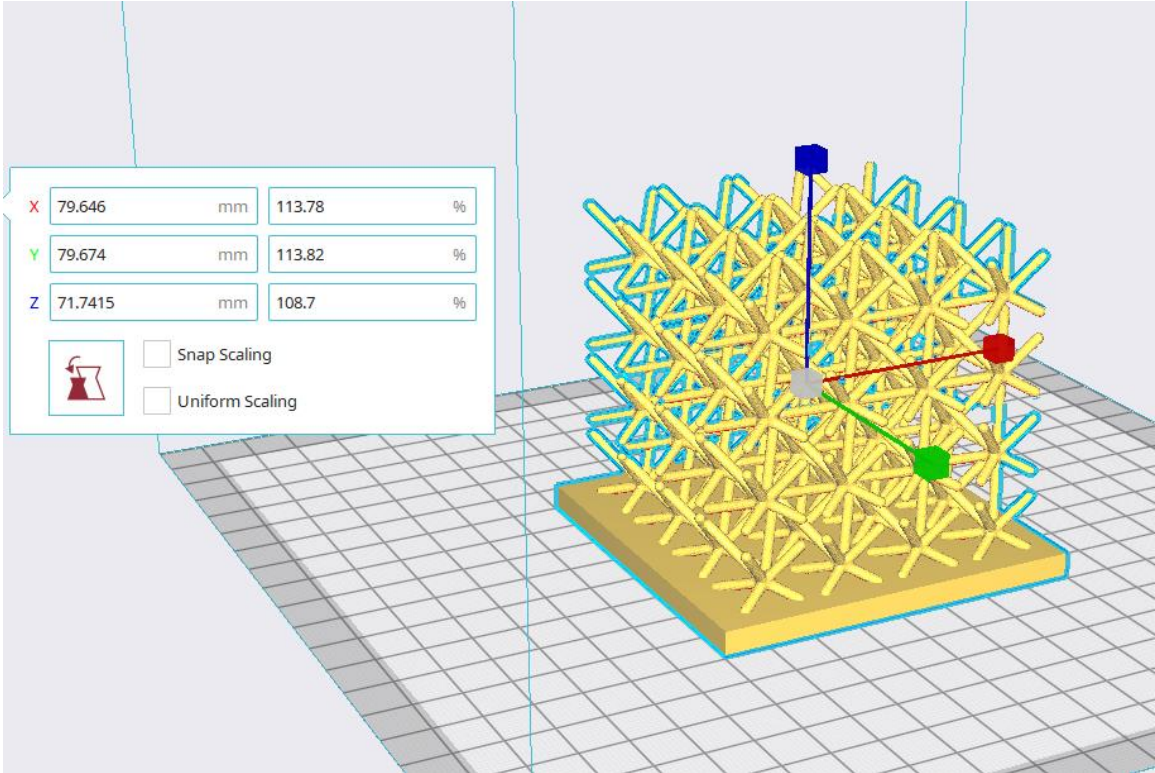


Figure 19: Scaled Heat Sink in Slicing Software

5.3 Microscopy Analysis

As mentioned, there are 4 states that the copper-infused filament experiences: raw filament, printed filament, debinded, and sintered. Microstructure analysis of the copper parts was done to evaluate part composition at all four stages. An energy dispersive spectroscopy (EDS) analysis and a scanning electron microscopy analysis (SEM) were used to evaluate the materials. The SEM analysis provides beautiful pictures that allow us to see the microstructure of the materials and how the copper and PLA interact. The SEM can numerically show us what the filament is made of and how much. The SEM scans are normalized to exclude small traces of other elements being picked up by the scan. The major components of the scan are scaled so that the total composition of the major components is 100%.

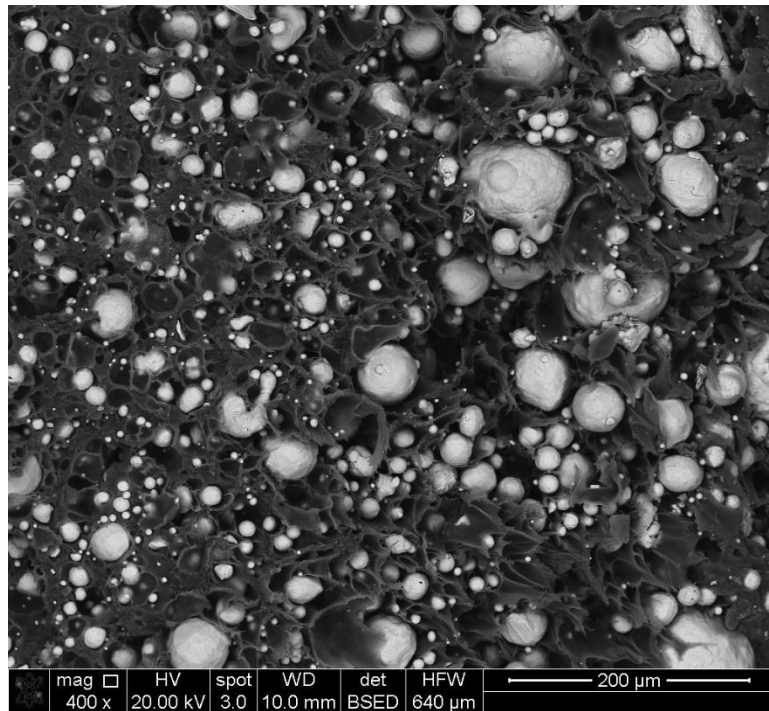


Figure 20: SEM Image of Copper Filament

The SEM scan of the raw filament in Figure 22 depicts the copper granules (shown in white) embedded in the PLA matrix. Without knowing the actual method used to manufacture the filament, it is likely some ratio of copper powder is mixed in with the polylactic acid and then extruded to make the filament. The high density of copper in the scan may be misleading since some of these heavy granules could have fallen out from the sample filament. There appear to be some craters where granules may have been nested before the image was taken. To account for this, a sample of raw filament was polished and analyzed with the SEM camera. As suspected the polished filament sample has a visibly higher density of copper.

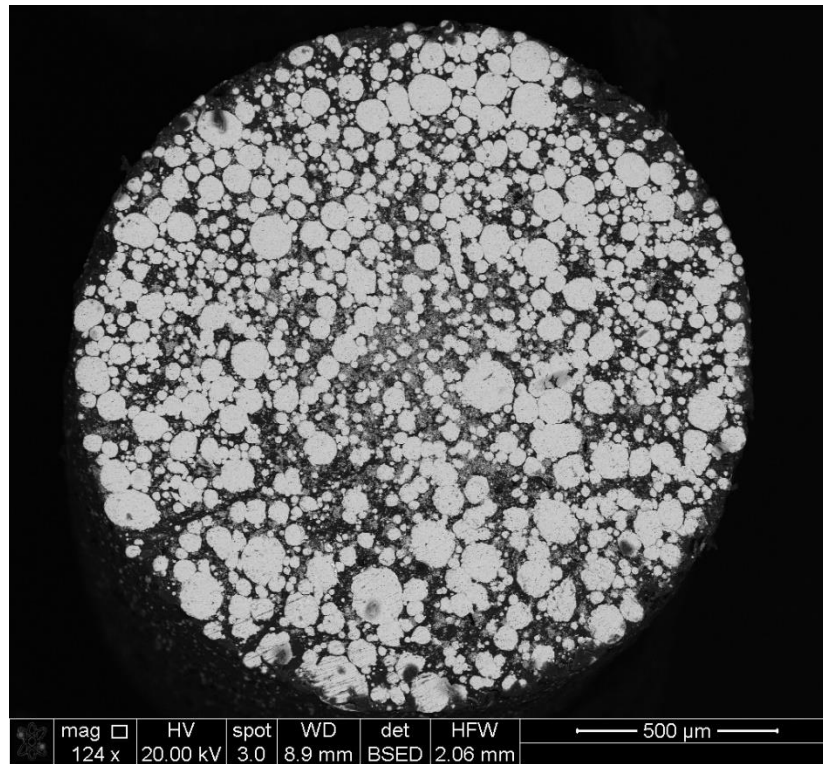


Figure 21: SEM Image of Polished Copper Filament

Comparing the debinded and sintered samples illustrates what is happening to the microstructure. From Figure 24 of the debinded sample and Figure 25 of the sintered sample, we can see that most of the PLA has been melted out of the part. However, the copper granules are still discrete and lightly bonded to each other. It's believed the dark fragment on the surface is the char after the sample was debinded. The parts were cleaned with a wire brush but remained charred in appearance. (Interestingly, the sintered parts cleaned better, likely due to a smoother surface having fewer features that might make it harder to remove the char). After sintering, the surface of the part has become smoother as the copper fused.

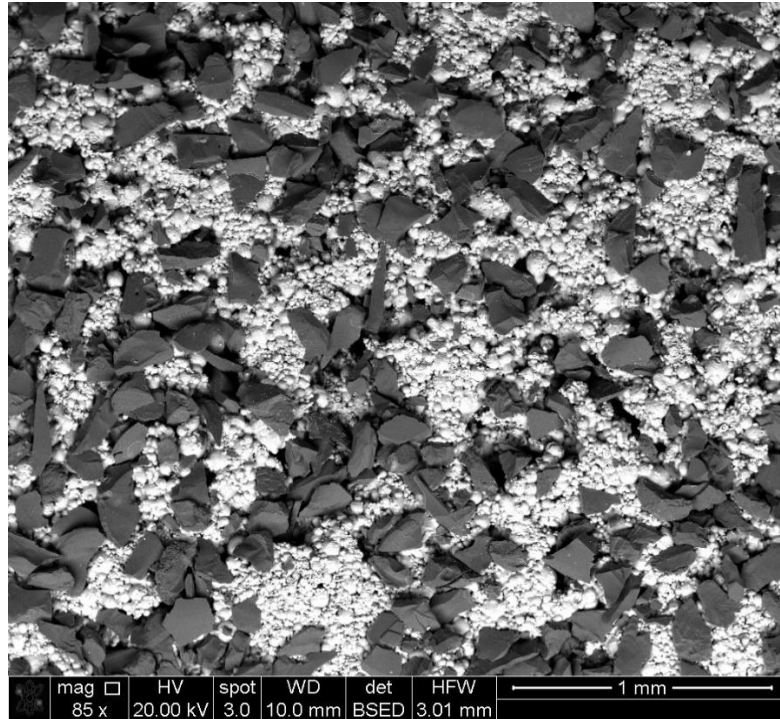


Figure 22: SEM Image of Debinded Copper Sample

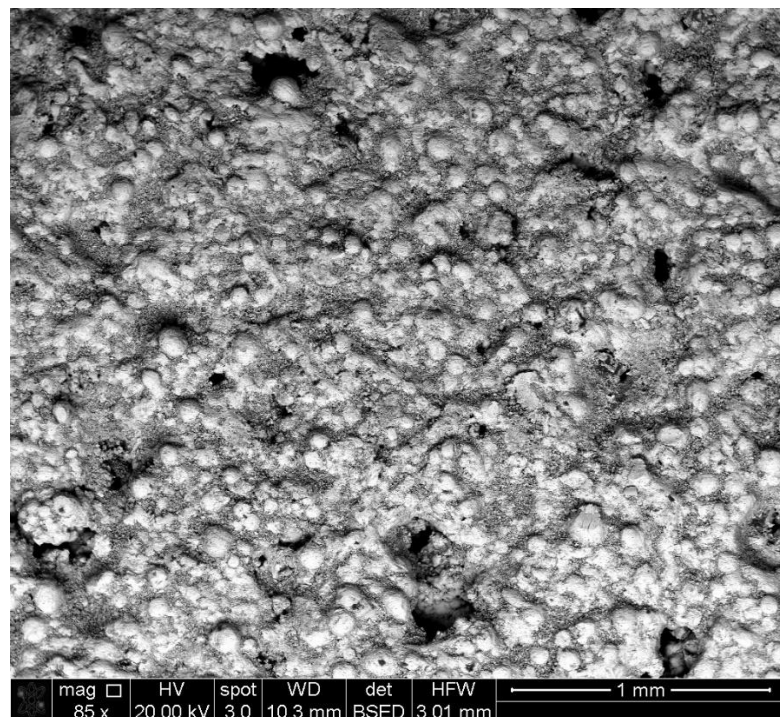


Figure 23: SEM Image of Sintered Copper Sample

From the EDS report, it was found that the sintered filament was composed of 82% copper. The next highest elements reporting was oxygen at 9% and carbon at just under 6%. The remaining composition of the materials included magnesium, aluminum, silicon, and chlorine. It is believed the oxygen could represent some feedback from the air as well as parts of the PLA along with the carbon. As for the remaining materials, they could be remnants from the de-binding and sintering materials used to pack the part in the crucible. After analyzing the normalized values, the study shows that the filament has a sufficiently high enough content of copper, along with a well-bonded structure to promote great internal conduction when used for heat sink applications.

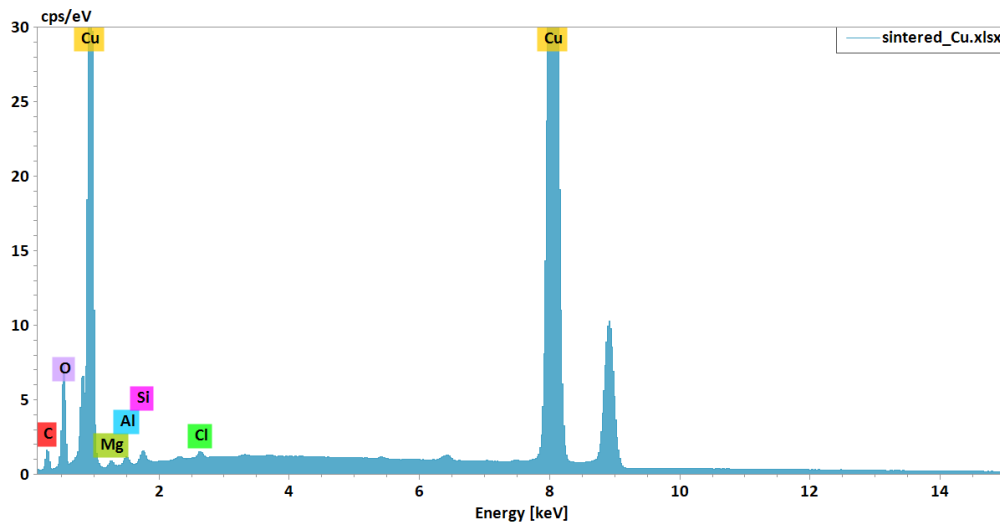


Figure 24: Graph of EDS Scan

Table 15: Results from EDS Scan

Element	At. No.	Mass [%]	Mass Norm. [%]	Atom [%]
Carbon	6	6.575392	5.936925352	20.21346
Oxygen	8	10.04345	9.068233493	23.17807
Magnesium	12	0.977079	0.882204835	1.484336
Aluminum	13	0.662734	0.598383074	0.906924
Silicon	14	0.585234	0.528408198	0.769389
Chlorine	17	0.095078	0.085846261	0.099022
Copper	29	91.8152	82.89999879	53.34879
		110.7542	100	100

CHAPTER VI

CONCLUSION

6.1 Conclusion

In this study, a set of lattice structures were investigated and optimized for heat sink applications using data obtained from computational fluid dynamics simulation imported into a design of experiments. The study analyzed 6 lattice structures with varying strut diameters and unit cell sizes. An in-depth microscopy analysis was performed on the copper-PLA infused filament and showed that the filament is a capable material to be used for heat sink applications. The CFD simulations provided data on the heat transfer, heat transfer coefficient, thermal resistance, and surface area of the lattice structures. After interpreting the results of the design of experiments, three optimizations with light, moderate and heavy constraints were performed on the structures. Our optimizations showed that the smaller strut diameter (limited by the capabilities of FDM manufacturing) was a key parameter for natural convection lattice structure heat sinks. We identified Netfabb's "W" unit cell as the optimal structure from our study for heat sink applications. We observed an interesting inversely proportional relationship between the surface area and heat transfer results. This phenomenon has also been observed by Dixit. Overall, our study identified trends of lattice structures for heat sink applications and verified them computationally. Our method of optimization was able to efficiently

analyze multiple heat sinks and reach 3 optimized lattice structures using a design of experiments. These lattice structures that have been designed for FDM show promising results as a low-cost solution for thermal management.

6.2 Future Work

The future work directly related to this research would be to experimentally validate the results of this optimization methodology. This work is underway but has been delayed due to lead times and a lack of available resources for manufacturing. Our research team has already worked on a peer-reviewed process of testing 3D-printed heat sinks and has testing materials ready when the parts are available.

We believe that the optimization methodology used in this study can be applied to other heat sinks beyond lattice structures. The design of experiments used in this study significantly reduced the labor of optimization and presented data in an easy-to-manage representation. Utilizing modeling tools like Netfabb and Star CCM+ quickly and accurately bypassed experimental optimization. This methodology could be applied to standard plate-fin heat sinks by choosing physical parameters like fin thickness, fin height, and fin gap while optimizing for the same responses. Beyond heat sinks, there is also an application for this methodology that could help any designer efficiently optimize parts by utilizing modern computational modeling tools.

While our research chose to focus on fused deposition modeling, selective laser sintering is also a very exciting process that could be investigated. As noted in this paper, our designs considered the manufacturing process and were constrained by what our FDM printer could produce. The rule of thumb when designing for FDM is that features should be no less than 2mm, which is why our study used this as a lower bound for strut

diameter. SLS has been known to be dimensionally accurate while printing features less than a millimeter. Using this technology could provide different results from the optimization. However as mentioned previously, copper is a very difficult material to use with SLS printers and could present additional challenges for experimental validation.

To further develop the methodology used in this study, supplying the ANOVA model with more data points should yield a higher accuracy optimization. Eighteen heatsinks were run in Star CCM+ to train our model. Once the initial conditions were set up for the CFD simulation, the only labor required was to replace the previous structure with the next one, create solid and fluid domains, and re-mesh. While some experience using CFD software was required, this is an efficient process. The ANOVA model could be built with more simulation data eventually yield higher accuracy results. The number of simulations entered in the model could then be optimized until the desired accuracy is reached.

Lattice structures are unique structures that all have different thermal and mechanical properties. Multifunctional optimization using the same methodology in this study would be a very intriguing area of research. In addition to the thermal responses from these structures, mechanical ones, like stress and deflection could characterize how the lattices perform in load-bearing conditions as well. Finite element analysis simulations could rapidly model these structures' mechanical properties. Load-bearing heat sinks offer promising applications in the aerospace industry where lightweight structures are required. Adding the capability of efficient heat dissipation to these structures further reduces the weight by eliminating the need for heat exchangers.

REFERENCES

- [1] C. Wang, Q. Lu, Y. Liu, H. Huang and J. Sun, "Progressive review of heat transfer enhancement technologies in 2010–2020," *Sustainable Energy Technologies and Assesments*, 2023.
- [2] heatsinkcalculator.com, "The importance of radiation in heat sink design".
- [3] T. Axsom, "Heat Sink Design Guide & Considerations," 2022.
- [4] D. Ashby, *Electrical Engineering 101 (Third Edition)*, Newnes, 2012.
- [5] P. West, "What's the best heat sink manufacturing process?," *Electronic Specifier*, 2022.
- [6] Advanced Thermal Solutions, "Heat Sink Manufacturing Technologies," Qpedia, 2010.
- [7] BOYD Corporation, "Boyd Heat Sink Fabrications Guide," 2021.
- [8] Z. Khattak, H. Ali, J. Ahmad and S. Shah, "PLATE FIN AND PIN FIN HEAT SINK VARIOUS DESIGNS ASPECTS, (REVIEW ON HEAT SINK COMPETENCE)," 2016.
- [9] Y. Joo and S. J. Kim, "Comparison of thermal performance between plate-fin and pin-fin heat sinks in natural convection,," *International Journal of Heat and Mass Transfer*, 2015.
- [10] Expert Market Research, "Global Heat Sinks Market Outlook," 2022.
- [11] F. P. Incropera,, D. P. DeWitt, T. L. Bergman and A. S. Lavine, *Fundamentals Of Heat And Mass Transfer 6h ed.*, New York: Wiley and Sons, 2007.
- [12] M. Ashby, "The Properties of foams and lattices," *Philisophical Transactions of the Royal Society A Mathematical, Physical and Engineering Sciences*, 2005.
- [13] L. Xiao, X. Xu, G. Feng, S. Li, W. Song and Z. Jiang, "Compressive performance and energy absorption of additively manufactured metallic hybrid lattice structures," vol. Volume 219, 2022.

- [14] W. Chanatry, "Design with a Purpose: Introduction into Lattice Structures," 2021.
- [15] M. Leary and et al, "Inconel 625 lattice structures manufactured by selective laser melting (SLM): Mechanical properties, deformation and failure modes," *Materials and Design*, pp. 179-199, 2018.
- [16] A. Alhammadi, "Microstructural characterization and thermomechanical behavior of additively manufactured AlSi10Mg sheet cellular materials," *Materials Science and Engineering A*, p. 139714, 2020.
- [17] L. Liu, "Investigation on numerical analysis and mechanics experiments for topology optimization of functionally graded lattice structure," *Additive Manufacturing*, p. 47, 2021.
- [18] S. Kechagias, R. N. Oosterbeek, M. J. Munford, S. Ghose and J. R. Jeffers, "Controlling the mechanical behaviour of stochastic lattice structures: The key role of nodal connectivity," vol. Volume 54, 2022.
- [19] A. Chaudhari, "Experimental investigation of heat transfer and fluid flow in octet-truss lattice geometry," *International Journal of Thermal Sciences*, pp. 64-75, 2019.
- [20] M. Leary, M. Mazur, J. Elambasseril, M. McMillan, T. Chirent, Y. Sun, M. Qian, M. Easton and M. Brandt, "Selective laser melting (SLM) of AlSi12Mg lattice structures," *Materials & Design*, 2016.
- [21] J. Ho, K. Leong and T. Wong, "Experimental and numerical investigation of forced convection heat transfer in porous lattice structures produced by selective laser melting," *International Journal of Thermal Sciences*, 2019.
- [22] T. Dixit, P. Nithiarasu and S. Kumar, "Numerical evaluation of additively manufactured lattice architectures for heat sink applications," *International Journal of Thermal Sciences*, 2021.
- [23] B. Redwood, F. Schoffer and B. Garret, *The 3D Printing Handbook: Technologies, design and applications*, 2018.
- [24] T. D. Ngo, A. Kashani, G. Imbalzano, K. T. Nguyen and D. Hui, "Additive manufacturing (3D printing): A review of materials, methods, applications and challenges," *Composites Part B: Engineering*, 2018.
- [25] X. Tian, A. Todoroki, T. Liu, L. Wu, Z. Hou, M. Ueda, Y. Hirano, R. Matsuzaki, K. Mizukami, K. Iizuka, A. V. Malakhov, A. N. Polilov, D. Li and B. Lu, "3D Printing of Continuous Fiber Reinforced Polymer Composites: Development, Application, and Prospective," *Chinese Journal of Mechanical Engineering: Additive Manufacturing Frontiers*, 2022.
- [26] T. Maconachie, M. Leary, B. Lozanovski and X. Zhang, "SLM lattice structures: Properties, performance, applications and challenges," *Materials and Design*, vol. 183, p. 108137, 2019.
- [27] A. Evans and et al, "The topology design of multifunctional cellular metals," *Progress in Materials Science*, vol. 46, pp. 309-327, 2001.
- [28] T. Maconachie, M. Leary, B. Lozanovski and X. Zhang, "SLM lattice structures: Properties, performance, applications and challenges," *Materials and Design*, p. 108137, 2019.

- [29] B. Michele and et al, "Development of a multifunctional panel for aerospace use through SLM," *11th CIRP Conference on Intelligent Computation in Manufacturing Engineering, CIRP ICME '17*, pp. 215-220, 2018.
- [30] J. Zhou and et al, "On the deformation of aluminum lattice block structures: from struts to structures," *Mechanics and Materials*, pp. 723-737, 2004.
- [31] D. Jang, S.-J. Park, S.-J. Yook and K.-S. Lee, "The orientation effect for cylindrical heat sinks with application to LED light bulbs," *International Journal of Heat and Mass Transfer*, 2014.
- [32] D. Carne, "Design Optimization Methods for Additively Manufactured Natural Convection Heatsinks," ProQuest, 2021.
- [33] L. Fratolocchi, "Adoption of 3D printed highly conductive periodic open cellular structures as an effective solution to enhance the heat transfer performances of compact Fischer-Tropsch fixed-bed reactors," *Chemical Engineering Journal*, p. 123988, 2020.
- [34] X. Hu, "Experimental study on the thermal response of PCM-based heat sink using structured porous material fabricated by 3D printing," *Case Studies in Thermal Engineering*, p. 100844, 2021.
- [35] T. Lu, "Active cooling by metallic sandwich structures with periodic cores," *Progress in Materials Science*, pp. 789-815, 2005.
- [36] S. Yun, "Numerical analysis on thermo-fluid–structural performance of graded lattice channels produced by metal additive manufacturing," *Applied Thermal Engineering*, p. 117024, 2021.
- [37] H. Yan, Q. Zhang, W. Chen, G. Xie, J. Dang and T. J. Lu, "An X-lattice cored rectangular honeycomb with enhanced convective heat transfer performance," *Applied Thermal Engineering*, vol. Volume 166, p. 114687, 2020.
- [38] B. Vaissier, J.-P. Pernet, L. Chougrani and P. Véron, "Parametric design of graded truss lattice structures for enhanced thermal dissipation," *Computer-Aided Design*, vol. Volume 115, pp. 1-12, 2019.
- [39] T. D. Munusamy, S. Y. Chin and K. Md.Maksudur Rahman, "Photoreforming hydrogen production by carbon doped exfoliated g-C₃N₄: Optimization using design expert®software," *Materials Today: Proceedings*, 2022.
- [40] N. Sakthivel, J. Bramsch, P. Voung, I. Swink, S. Averick and H. Vora, "Investigation of 3D-printed PLA–stainless-steel polymeric composite through fused deposition modelling-based additive manufacturing process for biomedical applications," *Medical Devices & Sensors*, 2020.
- [41] S. S. S. S. Paramasivam, L. D. Sawant, H. Natarajan, U. Sumanth and K. P. Singh, "Numerical simulation process parameter optimization in metal additive manufacturing for getting better quality of products," *Materials Today: Proceedings*, 2022.
- [42] W. Kenton, "Analysis of Variance (ANOVA) Explanation, Formula, and Applications," 2022.
- [43] S. D. I. Software, "Simcenter STAR-CCM+," 2023.
- [44] J. Hunter, "Matplotlib: A 2D graphics environment," vol. 9, 2007.

- [45] K. J. Maloney, "Multifunctional heat exchangers derived from three dimensional micro-lattice structures," *International Journal of Heat and Mass Transfer*, pp. 2486-2493, 2012.

VITA

Turner Mark McCoy

Candidate for the Degree of

Master of Science

Thesis: A PARAMETRIC OPTIMIZATION OF LATTICE STRUCTURE HEAT
SINKS: AN INTEGRATED COMPUTATIONAL AND EXPERIMENTAL
APPROACH

Major Field: Engineering Technology

Biographical:

Education:

Completed the requirements for the Master of Science in Engineering
Technology at Oklahoma State University, Stillwater, Oklahoma in May, 2023.

Completed the requirements for the Bachelor of Science in Mechanical
Engineering Technology at Oklahoma State University, Stillwater, Oklahoma in
2021.

ProQuest Number: 30485108

INFORMATION TO ALL USERS

The quality and completeness of this reproduction is dependent on the quality and completeness of the copy made available to ProQuest.



Distributed by ProQuest LLC (2023).

Copyright of the Dissertation is held by the Author unless otherwise noted.

This work may be used in accordance with the terms of the Creative Commons license or other rights statement, as indicated in the copyright statement or in the metadata associated with this work. Unless otherwise specified in the copyright statement or the metadata, all rights are reserved by the copyright holder.

This work is protected against unauthorized copying under Title 17, United States Code and other applicable copyright laws.

Microform Edition where available © ProQuest LLC. No reproduction or digitization of the Microform Edition is authorized without permission of ProQuest LLC.

ProQuest LLC
789 East Eisenhower Parkway
P.O. Box 1346
Ann Arbor, MI 48106 - 1346 USA